Published in final edited form as:
Prog Retin Eye Res. 2012 September ; 31(5): 442–466. doi:10.1016/j.preteyeres.2012.05.002.

Speed, sensitivity, and stability of the light response in rod and cone photoreceptors: Facts and models

Juan I. Korenbrot
Department of Physiology, School of Medicine, University of California San Francisco

Abstract

The light responses of rod and cone photoreceptors in the vertebrate retina are quantitatively different, yet extremely stable and reproducible because of the extraordinary regulation of the cascade of enzymatic reactions that link photon absorption and visual pigment excitation to the gating of cGMP-gated ion channels in the outer segment plasma membrane. While the molecular scheme of the phototransduction pathway is essentially the same in rods and cones, the enzymes and protein regulators that constitute the pathway are distinct. These enzymes and regulators can differ in the quantitative features of their functions or in concentration if their functions are similar or both can be true. The molecular identity and distinct function of the molecules of the transduction cascade in rods and cones are summarized. The functional significance of these molecular differences is examined with a mathematical model of the signal-transducing enzymatic cascade. Constrained by available electrophysiological, biochemical and biophysical data, the model simulates photocurrents that match well the electrical photoresponses measured in both rods and cones. Using simulation computed with the mathematical model, the time course of light-dependent changes in enzymatic activities and second messenger concentrations in non-mammalian rods and cones are compared side by side.

Keywords

Photoreceptors; ion channels; Calcium; cGMP; transduction; retina; rod; cone; mathematical models

In the dark, rod and cone photoreceptors of the vertebrate retina sustain a circulating ionic current that flows along the extracellular space from the inner to the outer segment (Hagins et al., 1970). The circulating current is an outward K^+ ion flux across the inner segment membrane mediated by voltage-gated K^+ channels (Bader et al., 1982; Hestrin, 1987; Barnes and Hille, 1989; Maricq and Korenbrot, 1990a, b) and an inward Na^+ and Ca^{2+} ion flux across the outer segment membrane mediated by cyclic nucleotide-gated ion channels (CNG channels) (Fesenko et al., 1985; Yau and Nakatani, 1985a). Light suppresses this current by closing the outer segment CNG channels and, as a consequence, the cell membrane potential hyperpolarizes (Baylor and Fuortes, 1970; Tomita, 1971; Baylor and Hodgkin, 1973; Schwartz, 1973) initiating the process of vision.

Correspondence Juan I Korenbrot, juan.korenbrot@ucsf.edu, Telephone 1-415-789-8734.

The functional features of the light response of rods and cones are well suited to the ecological needs of vertebrate behavior. Thoroughly dark adapted rods yield a detectable signal, a signal larger than their intrinsic noise, when only a single visual pigment molecule is excited by light (Baylor et al., 1979b) while cones yield a detectable signal only when light flashes excite 4 to 10 visual pigment (VP) molecules per cell (Naarendorp et al., 2010; Koenig and Hofer, 2011; Korenbrot, 2012b). Cones adjust their photosensitivity as a function of mean background intensity, and thus can respond to changes over 9 log units of light intensity, the range of illuminance from a clear night sky (2×10^{-3} lux) to that by direct sunlight (1.3×10^{5} lux) (Wikipedia.org). Rods, however, adapt over a smaller range of light intensities than do cones (Baylor et al., 1984; Fain et al., 1989; Matthews et al., 1990; Schnapf et al., 1990). Indeed, under bright steady illumination the outer segment dark current can be fully suppressed in rods (response saturation), but not in cones (response cannot be saturated) (Jones et al., 1993; Burkhardt, 1994; Kenkre et al., 2005). In cones, extremely intense steady light suppresses the circulating current for only a brief moment and it then recovers to a new steady value, reflecting reopening of the CNG channels. In human cones, for example, when over 90% of the visual pigment (VP) is bleached, the dark current amplitude is only half that measured in the dark (Kenkre et al., 2005) and the same is observed in cones of non-mammalian species (Jones et al., 1993).

Over the first six log units of light intensity above threshold, cones respond with constant contrast. That is, flashes of a given intensity measured as a percentage of the background intensity generate the same amplitude response regardless of the absolute magnitude of the background light (Normann and Werblin, 1974; Normann and Perlman, 1979; Burkhardt and Gottesman, 1987; Burkhardt, 1994). This feature allows cones to respond over about two log units of light intensity centered on the background level, regardless of the absolute background intensity (Burkhardt and Gottesman, 1987; Perlman and Normann, 1998). This is also the range of intensities relative to the mean background level typical of natural scenes (Mante et al., 2005). The time course of the light response is faster in cones than in rods, and can inform of changes in illuminance as frequent as every 100–200 msec, for example, the interval between eye saccades typical in language reading (Blythe et al., 2006). The chromatic range of the cone response, summed over the absorbance spectra of all known cone opsins (with peak absorbance ranging from 360 nm to 630 nm) is well tuned to the solar spectral irradiance on earth's surface, a spectrum that ranges from 220 nm to 2400 nm with a single peak at 500 nm (Thuilier et al., 2003).

Rod and cone photoresponses differ in any given vertebrate species, yet both are extremely stable and reproducible. This reflects the exceptional regulation of the cascade of enzymatic reactions that link VP excitation by light to the gating of the CNG ion channels. This enzymatic transduction pathway accomplishes the same task in both receptor types but with different speed, photosensitivity and light and dark adaptation features. The extensive biochemical and biophysical information on the transduction pathways in rods and cones can be difficult to reduce into a single coherent view. Mathematical models offer a succinct and precise tool to describe and understand physiological processes based on the function of the molecules that constitute the processes. Starting with the pioneering mathematical models of phototransduction by Tranchina and Sneyd in cones (Sneyd and Tranchina, 1989; Tranchina et al., 1991) and Forti et al. in rods (Forti et al., 1989; Torre et al., 1990), ever improving, coherent models of phototransduction have evolved to include new and refined biochemical and biophysical information. A number of contemporary models have been developed that quantitatively describe the full complement of reactions involved in the phototransduction pathway. Among them are: rods (Pugh and Lamb, 1993; Hamer et al., 2003; Hamer et al., 2005; Caruso et al., 2010; Shen et al., 2010); cones (Reingruber and Holcman, 2008; Soo et al., 2008; Korenbrot, 2012b). These models share many specific features and generally address either rod or cone phototransduction. In this review, we

explore quantitative differences and similarities between the biochemical and biophysical reactions of the phototransduction pathways in rods and cones. We compare and contrast the differences and similarities using the same, comprehensive mathematical model of phototransduction (Korenbrot, 2012a). This model evolves from, and incorporates many features common to preceding models and adds recently discovered regulatory events, particularly with respect to feedback control by cytoplasmic Ca^{2+}. The efficacy of the model and the functional significance of many of the molecular differences between the rods and cones are verified by matching simulated and experimental photocurrents measured in dark-adapted photoreceptors.

Brief overview of the evolution of the signal transduction pathway of vertebrate photoreceptors

Evolution of the eye can now be traced from ancient multicellular organisms, related to corals and jellyfish, to humans (Schwab, 2011), but evolution of the retinal photoreceptors transduction pathway is not exclusively associated with the eye (reviewed in (Lamb et al., 2009). Rods and cones are but one example of ciliated sensory neurons that use the ancient cGMP (or cAMP) intracellular signal transduction pathway, a pathway associated with CNG ion channels from its very origin (Johnson and Leroux, 2010; Plachetzki et al., 2010). The structural homology of cGMP-gated ion channels and opsins across the genome of many species suggests the cGMP transduction pathway began with CNG ion channel functionally linked to non-opsin G protein coupled receptor protein (GPCR), which only later gained light sensitivity by the evolution of ancestral GPCR into animal opsins (Fredriksson et al., 2003; Plachetzki and Oakley, 2007; Plachetzki et al., 2010). Indeed, an opsin-CNG channel transduction pathway has been found to operate in *Hydra,* an ancient animal in the same phylum as corals anemones and jellyfishes. In *Hydra* blocking CNG channel conductance with the drug *l*-cis diltiazem abolishes a stereotyped light-driven behavior (Plachetzki et al., 2010).

Signal transduction takes place in the outer segment of rods and cones, which are highly evolved non-motile cilia characterized by an axoneme with a centriole-derived basal body and an elaborate intra-ciliary network of microtubulular fibrils that support an intraflagellar transport system (IFT) (reviewed in (Insinna and Besharse, 2008; Sung and Chuang, 2010). In the evolution of animal photoreceptors two classes of cells, ciliary and rhabdomeric, diverged from a common progenitor. These two photoreceptor classes are distinguished by their structure and are each commonly associated with vertebrate and invertebrate species, respectively. However, recent analysis shows that the two classes of photoreceptors are each associated with a distinct class of opsin molecules and transduction pathways rather than animal phyla (Plachetzki et al., 2005); (Arendt, 2003; Fain et al., 2010). Rhabdomeric opsin signaling is expressed in retinal ganglion cells and ciliary opsin signaling in invertebrates (Davies et al., 2010) (Nilsson and Arendt, 2008). The cilia-associated GPCR-CNG channel signaling pathway of vertebrate photoreceptors is found in phylogenetically diverse organisms (Johnson and Leroux, 2010). Particularly well understood are the GPCR-cyclic GMP (or AMP)-CNG ion channel pathways in ciliated sensory neurons of *C. elegans* (reviewed in (Bargmann, 2006) and ciliated olfactory neurons of vertebrates (reviewed in (Menini, 2010).

Functional consequence of the differences in rod and cone outer segment cytoarchitecture

The cytoarchitecture of the outer segment is very different in non-mammalian rods and cones, although it is less remarkable among mammalian photoreceptors (reviewed in

(Borwein, 1981). In cones there is only one membrane, the plasma membrane that folds back and forth forming lamella and also envelopes these lamella over about half their perimeter (Fetter and Corless, 1987). In rods, in contrast, the plasma membrane forms lamella only over a very short length at the base of the outer segment. These lamella then separate from the plasma membrane forming collapsed, closed disks. The plasma membrane envelops the disks over the full length of the outer segment, but the discs remain electrically disconnected from the plasma membrane.

There are some recognized functional consequences of the structural difference between rod and cone outer segments. The optics in intact eyes direct light rays along a nearly straight line from the inner segment to the outer segments and along the outer segment length. VP molecules at the base of the outer segment absorb photons and, therefore, reduce the photon flux available to the VP at the outer segment's tip, a phenomenon known as self-screening. Because of their taper, there is less self-screening in cones than in rods. Also, the cone outer segment taper, coupled with the specific geometry of the inner segment, improves the optical performance of cone photoreceptor allowing the inner segment to focus light onto the outer segment (Harosi and Novales Flamarique, 2012).

cGMP diffuses along the outer segment length and, therefore, transduction and adaptation signals extend away from the physical site of photon capture (Hemila and Reuter, 1981; Lamb et al., 1981; Matthews, 1986; Gray-Keller et al., 1999). Because of the differences in their cytoarchitecture, cGMP spreads further along the length of a rod than a cone outer segments of the same diameter (Holcman and Korenbrot, 2004). Across all species, the spatial spread of cGMP at the peak of the dim light photocurrent is 3 to 5 μm in rod outer segments, regardless of their absolute size. In cone outer segments and regardless of their absolute dimensions, the cGMP spatial spread of cGMP at the peak of the dim light photocurrent is 0.7 to 1 μm (Holcman and Korenbrot, 2004; Wu et al., 2006).

Rods, but not cones, respond to single excited VP* molecules with remarkable reproducibility (Rieke and Baylor, 1998; Whitlock and Lamb, 1999). This reproducibility is surprising because of the expected stochastic variability in a sequence of events initiated by one molecule (Rh*), but which invokes the activity of many other proteins as well (GRK, PDE, GC etc.). A specific mechanism is necessary to explain the single photon response reproducibility. Two mechanisms have been considered in theoretical detail and they may well coexists since one does not necessarily invalidate the other. In one scheme SPR reproducibility follows from the fact that rhodopsin inactivates through a sequence of transitions, not as a single event (Rieke and Baylor, 1998; Hamer et al., 2003). A second scheme proposes that SPR reproducibility follows from the physical separation of discs from the plasma membrane. The diffusion of the cGMP signal from the disc surface to the plasma membrane creates a spatial homogeneity that erases memory of the spot on the membrane where the stimulus photon was captured and suppresses SPR variability (Caruso et al., 2010).

The signal transduction pathway in rods and cones

VP in rods (rhodopsin) and cones (cone opsin) are members of the family of GPCR proteins (G protein coupled receptors). Their structure consists of 7 transmembrane alpha-helical domains with a bound light absorbing chromophore, 11-cis retinal (Palczewski, 2006; Park et al., 2008). Photon absorption initiates a sequence of conformational changes, each characterized by a distinct absorption spectrum in the visible range; the conversion rate from one state to another is temperature dependent. The conformational state that activates the transduction enzymatic pathway, Meta-II, first appears at room temperature about 1 msec after photon absorption. The sequence and thermal rates of conversion of various VP*

photo-intermediates between the dark state and Meta-II are quite similar in rod and cone visual pigments, regardless of their wavelength of maximum absorbance (Imai et al., 1995, Yoshizawa, 1994 #26102; Imai et al., 1997; Vought et al., 1999; Kusnetzow et al., 2001).

The active VP* state, as long as it exists, repeatedly collides with inactive heterotrimeric G protein molecules. The photoreceptor specific G protein, transducin, exist in the dark as a heterotrimer with bound GDP: Tαβγ-GDP. Upon collision with VP*, an active transducin state, T*, is generated by the exchange of GDP for GTP and dissociation into separate Tα-GTP and a Tβγ subunits (reviewed in (Chen, 2005; Downs et al., 2006; Shichida and Morizumi, 2007). Transducin molecules in rods (GNAT1) and cones (GNAT2) are distinct from each other (Lerea et al., 1986; Lerea et al., 1989). Molecular details of the interaction between Meta-II-rhodopsin and rod-transducin continue to be illuminated through recent studies of protein crystal structure (Noel et al., 1993; Sondek et al., 1994; Sondek et al., 1996; Scheerer et al., 2008; Jastrzebska et al., 2010; Choe et al., 2011). Comparable structural studies do not exist for the cone-specific opsins. Nonetheless, genomic analysis shows that the functional domains in opsin, those that interact with the relevant enzymes of the transduction cascade, are nearly the same in all vertebrate rods and cones (Carleton et al., 2005).

Tα-GTP, for as long as it exists, collides with inactive cGMP-specific phosphodiesterase (PDE6) and generates an active state, PDE*, that catalyzes the hydrolysis of cyclic GMP (Zhang and Cote, 2005; Lugnier, 2006; Conti and Beavo, 2007). Inactive PDE is a tetramer consisting of two catalytic subunits and two inhibitory subunits. The catalytic subunits are distinct in rods (PDEα and PDEβ) and cones (PDEc) (Gillespie and Beavo, 1988; Zhang and Cote, 2005; Muradov et al., 2010). The inhibitory subunits, PDEγ are also different in rods and cones. The enzymatic catalytic rate (k_{cat}) and substrate sensitivity (K_m) of each rod PDEα, rod PDEβ and cone PDEc subunits are essentially the same (Muradov et al., 2010). In native rod and cone outer segment membranes, one Tα-GTP molecule effectively relieves PDEγ inhibition at one PDE6 site and this leads to one-half of the maximal PDE activity; two Tα-GTP molecules are necessary to elicit maximal activation (Liu et al., 2009; Muradov et al., 2010). That is, one Tα-GTP activates one of the two catalytic subunits in the holo-PDE dimer and this yields the visual-pigment activated PDE*. PDE* has the enzymatic efficiency (kcat/Km) of one PDE subunit (PDEα or PDEβ or PDEc) because the probability that two Tα-GTP will activate the same PDE multimer and, therefore activate both α and β (in rods) or both c subunits (in cones) is very small.

PDE* hydrolyzes cyclicGMP as long as it remains active. The lifetime of PDE* is controlled by the dynamics of VP* **or** T* inactivation, depending on photoreceptor type and light-intensity (details below). VP* inactivates because it is phosphorylated by photoreceptor-specific opsin-kinase. Opsin-kinase is a member of the large family of GRK (G-coupled receptor kinase) and two specific homologs have been identified in photoreceptors: GRK1 and GRK7. GRK1 is expressed in all rods, but it is also expressed in cones of some species, for example, mice and rats (Weiss et al., 2001). GRK expression in cones, on the other hand, is heterogeneous. GRK7 is expressed in all cones, except in mice and rat cones, which do not have the GRK7 gene (Hisatomi et al., 1998; Chen et al., 2001; Weiss et al., 2001). In some species, pigs and dogs for example, only GRK7 is expressed in the cones. In most species, however, cones coexpress GRK1 and GRK7: zebrafish, carp (Weiss et al., 2001; Rinner et al., 2005; Tachibanaki et al., 2005; Wada et al., 2006), monkeys and humans (Chen et al., 2001; Weiss et al., 2001).

Both cone and rod VP* have 6 to 7 consensus phosphorylation sites in their cytoplasmic carboxy terminus, depending on species. VP* is progressively less able to activate transducin as the number of sites actually phosphorylated increases (Hurley et al., 1998;

Mendez et al., 2000; Kennedy et al., 2004). Phosphorylated-VP*, however, fully ceases to activate transducin only when it interacts with arrestin-1, a protein that binds the cytoplasmic surface of phosphorylated VP* and prevents any further interaction between VP* and transducin (reviewed in (Gross and Burns, 2010; Gurevich et al., 2011). At least two sites on the rhodopsin cytoplasmic carboxy terminus must be phosphorylated to promote arrestin binding, and the functional characteristics of arrestin binding change as the number of phosphorylated sites increases (Vishnivetskiy et al., 2007). Rods and cones express distinct arrestin molecules (Zhu et al., 2002a; Zhu et al., 2002b), and there are two classes of cone arrestin, perhaps in different cone subtypes (Brown et al., 2010; Renninger et al., 2011).

T* inactivates because GTP bound to Tα hydrolyses to GDP, and Tα-GDP re-associates with Tβγ. The intrinsic GTPase activity of Tα-GTP is sluggish and this rate is accelerated by interaction of Tα-GTP with RGS9 (regulator of G protein signaling) {Hε, 1998 #18358}. In fact, Tα-GTP interacts with a multi-protein complex that includes, in addition to RGS9: R9AP (anchoring protein), Gβ5-long, Gβ5-short and γ PDE (Hu and Wensel, 2002; Grant et al., 2006; Wensel, 2008). The molecular identity of the regulators of Tα-GTP appears to be the same in rods and cones (Zhang et al., 2003; Zhang et al., 2006; Wensel, 2008). T* inactivation is rate limited by its catalytic interaction with the “RGS9” multi-protein complex of regulatory proteins (Burns and Pugh, 2010).

To terminate the photoresponse and restore the dark condition, PDE* is inactivated and cGMP is newly synthesized from GTP by membrane-bound guanylate cyclase (GC) (reviewed in (Pugh et al., 1997; Koch et al., 2002). GC activity is Ca-dependent: catalytic activity decreases as Ca^{2+} concentration rises (Lolley and Racz, 1982; Koch and Stryer, 1988; Dizhoor et al., 1994; Koch et al., 2002). Ca-dependence is mediated by the interaction of the membrane-bound GC with soluble, Ca^{2+} binding proteins (Lambrecht and Koch, 1991) named GC-activating proteins (GCAP) (Lambrecht and Koch, 1991; Dizhoor et al., 1995; Gorczyca et al., 1995). GC activity is higher in light than in darkness because illumination lowers cytoplasmic free Ca^{2+} concentration through a well-understood mechanism detailed below.

It is difficult to anticipate the identity of the GC and GCAP protein homologues expressed in any given photoreceptor. Unique GC molecules are expressed in rods (retGCR1 and retGCR2) and cones (retGCC) (Hisatomi et al., 1999; Takemoto et al., 2009). However, the pairing of GCAPs and GCs varies with photoreceptor type and species. In humans, for example, GCAP1, GCAP2, GC1 and GC2 are all expressed in both rods and cones, while GCAP3 is expressed exclusively in cones (Imanishi et al., 2002). Yet neither mice cones (nor rods) express GCAP3 (Imanishi et al., 2002). The cellular expression pattern of GCAPS is even more complex in non-mammals. In zebrafish, for example, there are 6 GCAP isoforms of distinct amino acid composition, including homologues of mammalian GCAP1, 2 and 3, and each cone subtype expresses a particular combination of GCAP molecules (Imanishi et al., 2002; Scholten and Koch, 2011). All GCAPs, nonetheless, are members of the same genomic family: they are myristoylated Ca/Mg-binding proteins of the EF-hand superfamily. GCAPs consist of four EF-hands; one does not bind metals while the other three can bind Ca^{2+} and Mg^{2+}. GC activation at low Ca^{2+} and its inhibition at high Ca^{2+} follow a cycle of Ca^{2+}/Mg^{2+} exchanges on GCAP. At low Ca^{2+}, Mg^{2+} binds three EF-hands and GCAP activates GC. When Ca^{2+} concentration raises, Ca^{2+} replaces Mg^{2+} in one of the three EF hands and this inhibits GC activity (Dizhoor and Hurley, 1999; Dizhoor et al., 2010).

Light- and Ca^{2+}-dependent changes in cytoplasmic cGMP concentration are translated into a membrane current through the activity of the cyclic GMP-gated (CNG) ion channels, the

only ion channels present in the outer segment plasma membrane (Cook et al., 1989; Karpen et al., 1992). The probability these channels are open or closed is directly controlled by the cytoplasmic cGMP concentration (Haynes et al., 1986; Zimmerman and Baylor, 1986; Matthews, 1987; Haynes and Yau, 1990; Picones and Korenbrot, 1994). Although the principal gating mechanism of cGMP is to change the open-to-close probability, CNG channels exhibit more than one open conductance state and cGMP also changes the absolute conductance of the open channels (Sesti et al., 1994; Bucossi et al., 1997). CNG channels are heteromeric aggregates of α and β subunits (Kaupp and Seifert, 2002; Biel and Michalakis, 2009). Rod channels are assembled from 3 CNGA1 subunits and 1CNGB1 (Weitz et al., 2002; Zheng et al., 2002; Zhong et al., 2002). Recent X-ray structural analysis of analogous regions in the structure of rod and cone channel subunits suggest that cone channels are assembled from 3 CNGA3 subunits and 1CNGB3 subunits (Shuart et al., 2011).

CNG channels are selectively permeable to cations over anions, but also select among mono and divalent cations (Picones and Korenbrot, 1992; Zimmerman and Baylor, 1992; Tanaka and Furman, 1993; Haynes, 1995). The channels are permeable to Ca^{2+} ions, but permeating Ca^{2+} also binds to specific sites in the open pore from which it can be displaced by the transmembrane voltage (Colamartino et al., 1991; Eismann et al., 1994; Haynes, 1995; Picones and Korenbrot, 1995). This complex permeation and binding interaction between Ca^{2+} ions and the channel is physiologically important because it defines the voltage-dependence of the cGMP-gated current (Zimmerman and Baylor, 1992; Wells and Tanaka, 1997; Ohyama et al., 2002). The relative Ca^{2+} to Na^{+} permeability is higher in cone than in rod CNG channels (Frings et al., 1995; Picones and Korenbrot, 1995). Because of this permeability difference, in physiological ionic solutions the fraction of the current carried by Ca^{2+} is about twice as large in cone as in rod CNG channels (Ohyama et al., 2000; Ohyama et al., 2002).

There exists only a single class of active ion transporters in the outer segment plasma membrane, Na^{+}/Ca^{2+}, K^{+} ion exchangers (Cervetto et al., 1989; Lagnado and McNaughton, 1991; Schnetkamp et al., 1991). These ion carriers transport Ca^{2+} out of the outer segment, against an electromotive force, driven by the thermodynamically favored Na^{+} influx. The Na^{+}/Ca^{2+}, K^{+} transporters (NCKX) are members of the superfamily of CaCA (Ca^{2+}/cation antiporter) transport proteins. Different homologues are expressed in rods (NCKX1) and cones (NCKX2) (reviewed in (Schnetkamp, 2004; Lytton, 2007). The ion transport rate is controlled by the intra and extracellular concentration of each of the transported ions, as well as membrane voltage. The cation dependencies of NCKX1 and NCKX2 (external K^{+}, external Na^{+}, internal Ca^{2+}) are very similar to each other (Sheng et al., 2000). In intact photoreceptors under voltage-clamp, Na^{+} and K^{+} concentrations are constant and the transporter rate is controlled only by the changing intracellular Ca^{2+} (Perry and McNaughton, 1993).

Cytoplasmic free Ca^{2+} in the outer segment is controlled by the dynamics of its influx (via CNG channels) and efflux (via the NCKX transporter), combined with the action of cytoplasmic Ca^{2+} buffers (Yau and Nakatani, 1985b; Miller and Korenbrot, 1987; Lagnado et al., 1992). In the dark, the rates of Ca^{2+} inflow and outflow are the same and cytoplasmic free Ca^{2+} concentration is constant. Light causes a decrease in outer segment free Ca^{2+} because illumination reduces Ca^{2+} influx as CNG channels close (Gray-Keller and Detwiler, 1994; Younger et al., 1996; Sampath et al., 1999). Since Na^{+}/Ca^{2+},K^{+} exchanger transport is itself controlled by cytoplasmic free Ca^{2+}, then as Ca^{2+} concentration decreases so does the transporter-mediated Ca^{2+} efflux. Under steady illumination, therefore, Ca^{2+} efflux soon becomes equal to the reduced influx and a new stationary condition is reached with a new steady, but lower Ca^{2+} concentration.

The light-dependent change in cytoplasmic Ca^{2+} controls the function of several molecules in the transduction pathway: the enzymatic velocity of GC and GRK, the cGMP-sensitivity of CNG channels and the transport rate of the $Na^{+}/Ca^{2+},K^{+}$ exchanger. Except for the ion exchanger, Ca^{2+} control is mediated by the function of soluble, Ca^{2+}-binding proteins that interact with the target protein. For GC, it is the GCAP proteins. For GRK it is recoverin (Kawamura et al., 1996; Sato and Kawamura, 1997; Tachibanaki et al., 2005). Recoverin is a myristoylated protein, member of the EF-hand superfamily (Gorodovikova et al., 1994; Kawamura et al., 1996; Kawamura and Tachibanaki, 2002); (Flaherty et al., 1993; Weiergraber et al., 2003). Recoverin has 4 EF hands, of which two bind Ca^{2+} each with different apparent affinity. At high Ca^{2+}, recoverin binds to GRK and is physically trapped between opsin and the kinase, thus preventing GRK from phosphorylating the VP (Ames et al., 2006). At low Ca^{2+}, recoverin does not bind to GRK and the enzyme can act on VP*.

The cGMP dependence of rod and cone CNG channel activity is Ca^{2+} dependent: the cGMP concentration that opens a given fraction of the channels is lowered as Ca^{2+} concentration decreases (Nakatani et al., 1995a; Sagoo and Lagnado, 1996; Rebrik et al., 2000; Rebrik and Korenbrot, 2004). This Ca-dependent modulation of ligand sensitivity depends on the interaction between the CNG channel protein and a Ca^{2+} binding, soluble modulator protein. The channel modulator in rods is calmodulin (Hsu and Molday, 1994; Gordon et al., 1995; Bauer, 1996), and CNG-modulin, a newly discovered protein in non-mammalian cones (Rebrik et al., 2012a). Search is underway for a mammalian homolog of CNG-modulin.

Animal models and methods to investigate rod and cone transduction pathways

To focus on quantitative details, rather than generalities, we review in detail the transduction pathway underlying flash responses of rods in tiger salamander (*Ambystoma tigrinum*) and single cones in striped bass (*Morone saxitilis*) as models of all rods and cones. References quoted are limited, in as much as possible, to these two species, even when comparable information exists for photoreceptors in other species. Electrophysiological and biophysical data in these two photoreceptors are rich, but biochemical data are not. On the other hand, extensive biochemical research has been conducted in rods of other amphibian (toad *Buffo* and frog *Rana*) and cones of other fish (carp *Cyprinus* and zebrafish *Danio*). Biochemical data measured in mammals are used only when not available for non-mammalian species to avoid unjustified parametric values. The need to mix data gathered in different species may well lead to some errors and approximations, but the rod cone differences are so remarkable that errors that will likely be corrected in the future are unlikely to change profoundly our current view.

Transduction signals have been measured in rods and cones of several mammals (Tamura et al., 1989; Nakatani et al., 1991; Zhang et al., 2003), including primates and humans (Baylor et al., 1984; Schnapf et al., 1990; Kraft et al., 1993; Schneeweis and Schnapf, 1999). The opportunity to create genetically modified rod and cone photoreceptors has also fomented studies in mice as animal models (Fu and Yau, 2007). It turns out, however, that mammalian and non-mammalian rods are rather similar in their transduction characteristics, once differences in temperature and the Q10 of enzymatic activities are accounted for (Baylor et al., 1983; Lamb, 1984). The features of cone photosignals, on the other hand, are far more diverse across species and can differ even within the same species depending on the opsin molecule they express. In striped bass, for example, there are single and twin cones that express different opsins, λmax 542 nm and 605 nm respectively, and the receptors differ in photosensitivity, in the waveform of their photocurrents and their light-adaptation features (Miller and Korenbrot, 1993a 25379).

Several voltage- and ligand-gated ion channels are present in the plasma membrane of rod and cone inner segments (rods: (Bader et al., 1982; Corey et al., 1984; Hestrin, 1987), cones(Maricq and Korenbrot, 1988, 1990a, b; Tatsukawa et al., 2005; Liu et al., 2006). The activity of these channels serves to control the photoreceptor membrane voltage and determines the features of their synaptic signal. The activity of these channels must be distinguished from that of the light-driven CNG channels, an objective met by measuring photocurrents under voltage clamp. Photocurrent kinetics are accurately measured in rods, even in the absence of voltage-clamp, with the use of suction electrodes that record outer segment currents excluding the inner segment (Baylor et al., 1979a). This technique is appropriate because the outer segment membrane capacitance is small (8.6 ± 1.3 pF in tiger salamander) (Miller and Korenbrot, 1994), and under physiological ionic solutions rod cGMP-dependent current amplitude is voltage-independent over the voltage range measured between darkness and light (−30 mV to −60 mV) (Baylor and Nunn, 1986; Miller and Korenbrot, 1994). The tiger salamander rod photocurrents shown here were measured under voltage clamp in the whole-cell mode using tight-seal electrodes in the “perforated” patch configuration (Horn and Marty, 1988; Miller and Korenbrot, 1994).

Accurate current kinetics in bass cones can only be measured under voltage clamp because the outer segment plasma membrane capacitance is large (58.1 ± 13.2 pF (Miller and Korenbrot, 1993b). Bass single cone photocurrents shown here were measured under voltage clamp in the whole-cell mode (Korenbrot, 2012a). However, the method suffers because of the loss of outer segment regulatory proteins by diffusion into the electrode lumen (Rebrik and Korenbrot, 1998, 2004). Photocurrents shown here were stable because they were recorded within 7–8 minutes after first attaining the whole cell mode (7–8 minutes).

Dark current noise and the thermal stability of visual pigments

The amplitude of the outer segment dark current (Table 1) is only 2–5% percent of the maximum possible value of this current in both rods and cones (Hestrin and Korenbrot, 1987; Cameron and Pugh, 1990; Rebrik and Korenbrot, 1998). Because the maximum probability of CNG channels being in their open state is about 87%, the full extent of the photocurrent reflects controlled changes in the probability of CNG channels being open between a few percent (in the dark) and zero. Although this makes the overall magnitude of the photocurrent small, it makes it extremely reliable: The statistical variance in the probability of channel opening, that is, the uncertainty that the channel is in fact open with the desired probability is least in the extremes, when the probability is either very small or very large (Picones and Korenbrot, 1994; Alvarez et al., 2002).

The amplitude of the dark current is not constant but fluctuates about a mean value. This statistical variance is referred to as current noise and is characterized by the amplitude and frequency of the fluctuations. The amplitude of dark current noise is critically important to determine photoreceptor light threshold: A light signal is detectable only if its amplitude exceeds that of the dark current noise. Photoreceptor dark current noise is caused by three different phenomena: 1) variance in the probability of open-to-close transitions of the CNG channel, 2) fluctuations in the enzymatic activity of phopsphodiesterase, and 3) spontaneous thermal activation of the VP. Noise due to channel stochastic behavior is of little physiological consequence because it is minimized, as discussed above, and it contributes to current noise only at frequencies much higher than the frequency of the photoresponse (Rieke and Baylor, 1996; Holcman and Korenbrot, 2005).

PDE enzymatic activity in the dark fluctuates about its mean value, causing variance in the cytoplasmic cGMP concentration. The current noise thus generated is continuous in time and its power spectrum is different from that of the light-dependent signal (Rieke and

Baylor, 1996, 2000; Holcman and Korenbrot, 2005). In rods, the rms amplitude of the PDE-generated current noise is small (~0.035 pA) (Baylor et al., 1980; Rieke and Baylor, 1996), much smaller than that of signals generated by excitation of a single rhodopsin molecule (~1 pA), which makes the single rhodopsin response (SRR) readily detectable (Baylor et al., 1979b; Yau et al., 1979b).

The membrane current signal generated by VP thermal bleaching is indistinguishable from that generated by light-activated VP*. In rods, therefore, dark current noise arises from the sum of the small continuous component due to fluctuating PDE activity, and discrete large events that arise from rhodopsin thermal bleaching (Baylor et al., 1980). The difference between SRR generated by heat and those generated by light is only in their frequency. Light events, of course, occur at a frequency determined by the rate of photon delivery (Whitlock and Lamb, 1999; Doan et al., 2006). The rate of thermal events is determined by temperature and the number of rhodopsin molecules per rod. In toad rods at room temperature, for example, 1 Rh (out of $3x10^9$) is bleached by heat every 50 sec (Yau et al., 1979a; Baylor et al., 1980; Vu et al., 1997).

The thermal stability of VP reflects the strength of the bond between the 11-cis-retinal chromophore and the opsin protein. Whether the VP is expressed in rods or cones, thermal stability decreases as the wavelength of maximum absorbance shifts from blue to red (Luo et al., 2011). In green cones, opsin (543 nm) is nearly as stable as rhodopsin (520 nm), but the estimated single opsin response is rather small (~0.08 pA in bass cones), much smaller than the PDE-generated current noise amplitude (~0.28 pA) (Rieke and Baylor, 2000; Holcman and Korenbrot, 2005). In green cones, hence, the dominant source of dark current noise is the fluctuation in PDE activity. Furthermore, it can be expected that a signal will be detected above noise only when at least 3 to 4 VP molecules are excited simultaneously (Holcman and Korenbrot, 2005). Indeed, the signal threshold in bass green cones is the simultaneous absorption of 4–7 photons (Korenbrot, 2012b).

Because red opsin is so much less stable than green or blue opsin (Luo et al., 2011), VP thermal activation is the dominant source of dark noise in red-sensitive cones (Rieke and Baylor, 2000; Sampath and Baylor, 2002). The red cone dark current noise is larger in amplitude than that of green cones; hence, red cones can be expected to be less photosensitive than green ones. In striped bass, for example, one class of red-sensitive twin cones are 40 times less light sensitive than the green cones (Miller and Korenbrot, 1993a). An elegant demonstration of the relation between opsin absorbance maximum and dark current noise and photosensitivity are experimental studies of Xenopus rods transformed to express human red cone opsin. The photoresponses are rod-like in waveform indicating cone opsin can commandeer the rod transduction enzymes, but they are less sensitive and much noisier than wild type rods indicating dark current noise and sensitivity are determined by the relatively unstable red cone opsin (Kefalov et al., 2003). Qualitatively similar findings have been made in transgenic mice rod photoreceptors expressing the green-sensitive cone opsin, except the cone opsin in these transgenic rods is much less stable than expected (Sakurai et al., 2007).

Outer segment circulating current and biochemical activity in the dark

Rod photoreceptors in the dark consume more energy than they do in the light calculated as the rate of ATP hydrolysis per sec (Okawa et al., 2008). This because sustenance of the circulating dark current requires the activity of ATP-dependent Na^+ pumps located in the inner segment plasma membrane (Hagins et al., 1970). Because in rods light fully suppresses the dark current more energy is consumed in the dark than the light. In cones, on the other hand, energy consumption in the dark is essentially the same as rods, but energy

consumption remains high in the light because the circulating current is never suppressed, even at light levels that bleach over 95% of the VP (Jones et al., 1993; Kenkre et al., 2005).

Cytoplasmic cGMP concentration in the dark

Values presented in the following sections, whether experimentally measured or taken from the literature, are specified in as much as possible for tiger salamander rods (or other non-mammalian rods) and striped bass single cones (or other non-mammalian cones). For convenience, however, they are referred to as rod or cone values, respectively. Citations also are not comprehensive, but limited to the non-mammalian rods and cones, if possible, and bass and tiger salamander photoreceptors preferably.

The amplitude of the outer segment dark current is a direct measure of the standing cytoplasmic free cGMP concentration. For both rods and cones, the relationship between current amplitude and cGMP concentration is experimentally known, therefore, dark cytoplasmic cGMP concentration can be calculated for any photoreceptor by measuring its dark current.

In both rods and cones the cGMP dependence of current amplitude is given by the Hill equation (reviewed in (Yau and Baylor, 1989):

$$\frac{I(cGMP,Ca)}{I_{max}}=\frac{[cGMP]^{n_{CNG}}}{[cGMP]^{n_{CNG}}+K_{cGMP}(Ca)^{n_{CNG}}} \tag{1.1}$$

where $I_{(cGMP,\ Ca)}$ is outer segment membrane current, I_{max} is its maximum possible value, $[cGMP]$ is cGMP concentration, n_{CNG} is a dimensionless parameter that denotes the cooperativity of cGMP in gating the CNG channels, and $K_{cGMP}(Ca)$ is the cGMP concentration at which current is half its maximum value.

The value of K_{cGMP} is invariant when measured in membrane fragments detached from salamander rod or bass cone outer segments (Picones and Korenbrot, 1992; Sagoo and Lagnado, 1996; Hackos and Korenbrot, 1997), but it is Ca-dependent in intact photoreceptors (Nakatani et al., 1995a; Sagoo and Lagnado, 1996; Rebrik et al., 2000). The quantitative features of this modulation are one of the most significant physiological differences between receptor types. In rods the modulation is small in extent and occurs only at very low Ca^{2+} concentration, whereas in cones it is much larger in extent and its Ca^{2+} sensitivity overlaps the concentration range of the lightdependent changes in outer segment free Ca^{2+}. In both bass cones and salamander rods the dependence of $K_{cGMP}(Ca)$ on Ca^{2+} is well described by:

$$K_{cGMP}(Ca)={}^{\min}K_{cGMP}+({}^{\max}K_{cGMP}-{}^{\min}K_{cGMP})\frac{Ca}{Ca+{}^{CNG}K_{Ca}} \tag{1.2}$$

where ${}^{\min}K_{cGMP}$ and ${}^{\max}K_{cGMP}$ are minimum and maximum values of $K_{cGMP}(Ca)$, Ca is cytoplasmic free Ca^{2+} concentration and ${}^{CNG}K_{Ca}$ is the Ca^{2+} concentration at which $K_{cGMP}={}^{\min}K_{cGMP}+\frac{{}^{\max}K_{cGMP}-{}^{\min}K_{cGMP}}{2}$. On average in bass single cones the values of ${}^{\min}K_{cGMP}$ and ${}^{\max}K_{cGMP}$ are 105 μM and 316 μM, respectively, and ${}^{CNG}K_{Ca}$ is 0.86 μM (Rebrik and Korenbrot, 1998; Rebrik et al., 2000). In contrast, in salamander rods ${}^{\min}K_{cGMP}$ and ${}^{\max}K_{cGMP}$ are 28 μM and 37 μM, respectively, and ${}^{CNG}K_{Ca}$ is 0.055 μM (Sagoo and Lagnado, 1996). The dependence is on a 1.4 power of Ca^{2+}. The same values are reported for frog rods (Nakatani et al., 1995b). Mean measured values of dark current amplitude and the inferred dark cyclic GMP concentrations are listed in Table 1.

cGMP metabolic flux in the dark

cGMP concentration in the dark is high because the nucleotide is continuously synthesized by GC. The concentration is constant because the rate of synthesis is equal and opposite the rate of hydrolysis by PDE active in darkness.

PDE enzymatic activity follows Michaelis-Menten kinetics and its Km is known in both rods (Leskov et al., 2000; Muradov et al., 2010) and cones (Gillespie and Beavo, 1988; Huang et al., 2004).

$$^{dark}V_{PDE} = \varepsilon_{dark} \frac{[cGMP]_{dark}}{[cGMP]_{dark} + {}^{cGMP}K_m} \tag{1.3}$$

where $^{dark}V_{PDE}$ is the PDE catalytic activity in the dark, $[cGMP]_{dark}$ is the free cytoplasmic cGMP concentration and $^{cGMP}K_m$ is the Michaelis-Menten constant.

$$\varepsilon_{dark} = \frac{k_{cat}{}^{dark}N*}{LV_{OS}} \tag{1.4}$$

k_{cat} is the enzymatic turnover rate per molecule, $N*$ is the number of active PDE* in darkness, L is Avogadro's number, V_{OS} is outer segment volume.

GC enzymatic activity is Ca^{2+}-dependent in both rods (Lolley and Racz, 1982; Koch and Stryer, 1988) and cones (Takemoto et al., 2009) and given in the dark by:

$$^{dark}V_{GC} = \left(\frac{V_{GC}^{\max}}{1 + \left(\frac{^{dark}Ca}{K_{Ca}} \right)^n} \right) \tag{1.5}$$

where $^{dark}V_{GC}$ is the GC catalytic velocity in darkness, $V_{GC}^{\max}$ is the maximum enzyme activity, ^{dark}Ca is the cytoplasmic free Ca^{2+} concentration in the dark, K_{Ca} is the Ca^{2+} concentration at which the enzyme activity is half its maximum value and n is a dimensionless parameter that denotes cooperativity.

In the analysis detailed here, we assigned ^{dark}Ca to be 0.4 μM in the bass cones and 0.6 μM in the salamander rods. These are near the mean values of free Ca^{2+} concentration measured in other non-mammalian rods (Korenbrot and Miller, 1989; Gray-Keller and Detwiler, 1994; McCarthy et al., 1994) and cones (Sampath et al., 1999; Leung et al., 2007) at circulating dark currents comparable to those of the bass cones and salamander rods.

$^{dark}V_{GC}$ and $^{dark}V_{PDE}$ are experimentally known for bass cones and tiger salamander rods. In the dark, when these photoreceptors are suddenly exposed to a membrane permeable PDE inhibitor, the circulating dark current increases in amplitude reflecting net cGMP synthesis by GC no longer opposed by the blocked PDE activity (Holcman and Korenbrot, 2005) (Hodgkin and Nunn, 1988). The rate of dark current change upon pharmacological block of PDE is a direct measure of the dark GC catalytic activity. The same enzymatic rates are measured for PDE and GC when the respective counter balancing enzyme is blocked (Hodgkin and Nunn, 1988). From the experimentally measured changes in dark current upon suppression of one enzyme or the other, we computed PDE enzymatic activity in the dark. To this end, we first converted the rate of current change to a rate of cGMP concentration change using text equation (1.1), enzymatic activity was then computed based on this rate, and the dark cGMP concentration known from dark current amplitude measured

immediately before the pharmacological perturbation (Table 1). ε_{dark} was thus known for each cell from experimental data, without the need to know the ${}^{dark}N*$ value.

Ca^{2+} influx and efflux in the dark

Ca^{2+} influx, is a constant fraction of the outer segment inward dark current, and is given by (in μM/sec when the current is measured in pA).

$$ {}^{in}J_{Ca} = \frac{I_{OS} P_f 10^6}{zFV_{OS} B_{uff(Ca)}} \tag{1.6}$$

where I_{OS} (pA) is the outer segment membrane current current, P_f is the fraction of the dark current carried by Ca^{2+}, z is Ca^{2+} valence, F is Faraday's constant, V_{os} is the outer segment cytoplasmic volume and $B_{uff(Ca)}$ is the cytoplasmic Ca^{2+} buffering capacity, defined below. P_f is significantly higher in cone than rod CNG channels (Ohyama et al., 2000; Ohyama et al., 2002)(Table 1). The Ca^{2+} influx in the dark is the solution of this equation when the outer segment current is the dark circulating current.

Ca^{2+} efflux, is mediated by the Na^+/Ca^{2+}, K^+ exchanger. The exchanger transport rate is controlled by the intra and extracellular concentrations of Ca^{2+}, Na^+ and K^+ as well as membrane voltage (Sheng et al., 2000); (Perry and McNaughton, 1993). Assuming light does not change the Na^+ and K^+ concentrations and under voltage-clamp, the exchanger-mediated Ca^{2+} efflux is controlled by cytoplasmic Ca^{2+} and given (in μM/sec) by:

$$ {}^{out}J_{Ca} = \frac{2^{out} I_{NCKX}^{\max} 10^6}{zFV_{OS} B_{uff(Ca)}} \left[\frac{Ca}{Ca + K_{Ca}^{exc}} \right] \tag{1.7}$$

where $I_{NCKX}^{\max}$ (in pA) is the maximum exchanger current and other terms are the same as in text equation (1.6). The term in the square parenthesis is the Ca^{2+} dependence of the Na^+/Ca^{2+} K^+ exchanger transport rate where Ca is free cytoplasmic Ca2+ in the dark is and K_{Ca}^{exc} is the Ca^{2+} concentration at which the transport rate is half its maximum value. Ca^{2+} efflux in the dark is the solution of this equation when Ca^{2+} is the cytoplasmic free Ca^{2+} in the dark.

Cytoplasmic Ca^{2+} buffer capacity, is a feature of all biological cells, but the quantitative characteristics of this function are known in detail in relatively few instances (reviewed in (Neher, 1995). The only study available on the subject in photoreceptors is in tiger salamander rods, an investigation that suggests there exist two instantaneous buffer systems, one of high affinity and low capacity that operates below 1 μM free Ca^{2+} and another of low affinity and high capacity that operates at higher Ca^{2+} levels (Lagnado et al., 1992). If buffer systems in cones are similar to those rods, and assuming buffer molecules instantaneously bind Ca^{2+} at single sites with conventional equilibrium kinetics, it can be stated that in both receptor types (Lagnado et al. 1992):

$$ Ca_{TotB} = \frac{C_{HA} Ca}{Ca + K_{HA}} + (B+1)Ca \tag{1.8}$$

where Ca is the free ion concentration, Ca_{TotB} is the total Ca^{2+} (free plus buffer bound), C_{HA} is the total concentration of the high affinity buffer of Michaelis-Menten constant K_{HA} and B is the buffer capacity of the low affinity buffer.

Ca^{2+} buffering capacity is the ratio of bound to free Ca^{2+}, a parameter frequently assigned a single value, but which, in fact, is a function of Ca^{2+}, the derivative of equation (1.8) (Berlin et al., 1994; Neher, 1995)

$$Buff(Ca)=\frac{dCa_{TotB}}{dCa}=\frac{C_{HA}K_{HA}}{(Ca+K_{HA})^2}+B+1 \tag{1.9}$$

Biophysical and biochemical processes in the light

Following is a mathematical narrative of the reactions in the light transduction pathway of salamander rods and bass single cones. The majority of the reactions and their mathematical representation are part of and consistent with recent models (Hamer, 2000; Hamer et al., 2005; Soo et al., 2008; Burns and Pugh, 2009; Shen et al., 2010; Korenbrot, 2012b; Reingruber and Holcman, 2008). The model used here enriches previous ones because it incorporates the known quantitative characteristics of all Ca^{2+}-dependent reactions in both rods and cones: GC enzymatic activity, GRK enzymatic activity, CNG channels ligand sensitivity, and Na^+/Ca^{2+} K^+ transport rate. The model serves as a tool to compare rod and cone transduction pathways in detail.

Time course of visual pigment activation and inactivation

The number and rate of delivery of photons define the rate of visual pigment activation into a state, *VP**, that interacts with transducin to initiate the phototransduction process. *VP** inactivates because opsin is phosphorylated by G protein-coupled receptor kinase (GRK) (Chen et al., 1995; Baylor and Burns, 1998). Complete and reproducible rhodopsin inactivation requires multiple phosphorylation of each molecule (Mendez et al., 2000). The time course of VP* inactivation is complex because GRK catalytic rate depend on the state of VP* phosphorylation: the rate of phosphorylation of additional sites depends on the number of sites already phosphorylated (Hurley et al., 1998).

The number of physiologically relevant VP* phosphorylation sites is controversial (Hamer et al., 2003; Caruso et al., 2010). Based on certain experimental results (Doan et al., 2006) discussed further below, we adopted 6 as the number of relevant phosphorylation sites. Because the efficiency of transducin activation decays rapidly as each site is phosphorylated (decays by about a factor of 2 for each added phosphate (Gibson et al., 2000), whether 4, 5 or 6 sites are phosphorylated is of relatively little consequence in the waveform of the rod or cone photocurrent simulations. Arrestin can only bind to phosphorylated VP* and only after arrestin binding are VP* and its phosphorylated products completely unable to activate transducin (Gross and Burns, 2010).

GRK adds phosphates one at a time at a rate γ_{nPi}, which depends on n_{Pi} the number of phosphorylated sites. Each phosphorylated state of VP* is identified as $VP^*_{n_{Pi}}$, where $0 \geq \cdot\cdot$ $n_{Pi} \cdot\cdot \leq 6$. Arrestin binds to phosphorylated VP* with rate μ_{nPi} and quenches the ability of VP* to activate transducin. Therefore, the rate of change of the number of VP* molecules with n_{Pi} phosphorylated sites is given by:

$$\frac{dVP_0^*(t)}{dt}=Phot(t)-\gamma_0 VP_0^*(t) \tag{2.1}$$

$$\frac{dVP_1^*(t)}{dt}=\gamma_0 VP_0^*(t)-(\gamma_1+\mu_1)VP_1^*(t) \tag{2.2}$$

.
.

$$\frac{dVP^*_{n_{Pi}}(t)}{dt} = \gamma_{n_{Pi}-1} VP^*_{b_{Pi}-1}(t) - (\gamma_{n_{Pi}} + \mu_{n_{Pi}}) VP_{n_{Pi}}(t) \tag{2.3}$$

where *Phot(t)* is the number of VP* molecules produced by stimulus photons, γ_{nPi} is the rate of phosphorylation of VP* with n_{Pi} phosphorylated sites and μ_{nPi} is the rate of arrestin-dependent quenching of phosphorylated-VP*.

The rate of VP* phosphorylation, γ_{nPi}, decreases exponentially as the number of phosphorylated sites increases:

$$\gamma_{(n_{Pi}+1)} = \gamma_{n_{Pi}} e^{-\omega\gamma} \tag{2.4}$$

where ω_γ is a constant. μ_{nPi} is assumed to increase linearly with the number of phosphorylated sites n_{Pi}. This is a simplification since experimental data shows at least two sites must be phosphorylated before arrestin binds phosphorylated Rh*.

$$\mu_{n_{Pi}} = n_{Pi}\mu_0 \tag{2.5}$$

The GRK catalytic activity is Ca^{2+}-dependent. The Ca^{2+} dependence of cone VP* phosphorylation rate is given by (our fit to the descriptive data) (Sato and Kawamura, 1997):

$$\gamma_0 = \gamma_{max}\left(0.1 + 0.9\left(\frac{1}{1+\frac{Ca}{{}^{\gamma}K_{Ca}}}\right)\right) \tag{2.6}$$

where γ_{max} is the maximum possible value of this rate and ${}^{\gamma}K_{Ca}$ is the Ca^{2+} concentration at which $\gamma_0 = 0.55\gamma_{max}$.

Time course of PDE activation and inactivation

VP* interacts with the G-protein transducin and generates *T** (Tα-GTP), an activated form of the G-protein. Ψ_{nPi} is a rate gain that specifies the number of T molecules activated per sec by one VP*, a value that declines with the number of phosphorylated sites in VP. The affinity between of VP* and T declines exponentially with approximately 2-fold decrease per phosphorylation (Gibson et al. 2000). Thus:

$$\Psi_{(n_{Pi}+1)} = \Psi_{n_{Pi}} e^{-\omega_{act}} \tag{2.7}$$

Where, again, n_{Pi} is the number of phosphorylated sites, between 0 and 6, and ω_{act} =0.69 is the rate of exponential decay, an experimentally known value (Gibson et al., 2000).

One T* activates one PDE subunit in the PDE holo-enzyme to produce light-activated PDE*. PDE* inactivates at a rate α_{PDE}, which is the same as the rate at which T* disappears. The time course of PDE* existence, therefore, is given:

$$\frac{dPDE*(VP*,t)}{dt} = \sum \Psi_{n_{Pi}} VP^*_{n_{Pi}} - \alpha_{PDE} PDE^*(t) \tag{2.8}$$

T* disappearance requires its interaction with a multi-protein complex that includes: RGS9, R9AP, Gβ5L and γPDE (reviewed in (Wensel, 2008). The best present model of this

complex interaction posits that T* and PDE* form a single T*-PDE* molecular unit that interacts with a second molecular unit, composed of a multi-protein assembly of regulatory enzymes referred to as “RGS9” (reviewed in (Burns and Pugh, 2010). The RGS9 complex catalytically facilitates the conversion of the T*-PDE* unit into inactive T and PDE states. Inactivation of T*, hence, reflects two kinetic processes: the catalytic action of the “RGS9” complex and the intrinsic transducin GTPase activity. Either could be rate limiting. Which is the rate limiting event has been tested experimentally by investigating the effects of varying RGS9 concentration in transgenic mice rods (Burns and Pugh, 2009). Because the rate of photocurrent inactivation in rods changes with RGS9 concentration (Burns and Pugh, 2009), it has been proposed that in rods the rate limiting event is the rate of formation of the T*-PDE*-“RGS9” multimer and not the rate of GTPase hydrolysis characteristic of Tα-GTP. That is, the rate of formation of the T*-PDE*-“RGS9” complex is slower than the rate of GTP hydrolysis and, therefore, it is the event that determines the speed of PDE* (and T*) disappearance (reviewed in (Burns and Pugh, 2010). Comparable experiments are not yet been conducted in cones, but the same model will be applied.

Time course of light-dependent changes in cytoplasmic Ca^{2+} and GC activity

The rate of activation and inactivation of GC activity faithfully tracks the light-dependent changes in cytoplasmic free Ca^{2+}. To define the time course of changes in GC activity, therefore, the time course of changes in cytoplasmic free Ca^{2+} must be described.

Ca^{2+} concentration changes when the outer segment Ca^{2+} influx and efflux are not the same. That is,

$$\frac{dCa(t)}{dt} = {}^{in}J_{Ca} - {}^{out}J_{Ca} \tag{2.9}$$

From text equations (1.6) and (1.7)

$$\frac{dCa(t)}{dt} = \frac{I(t)P_f 10^6 - 2^{out}I_{NCKX}^{\max}\left(Ca/\left(Ca+K_{Ca}^{exc}\right)\right)10^6}{zFV_{COS}Buff(Ca)} \tag{2.10}$$

Integration of text equation (2.10), yields the time course of free Ca^{2+} concentration change, $Ca(t)$. The time course of GC activity changes is given by:

$$V_{GC} = (Ca(t)) = \left(\frac{V_{GC}^{\max}}{1+\left(\frac{Ca(t)}{{}^{GC}K_{Ca}}\right)^{n_{GC}}}\right) \tag{2.11}$$

where $V_{GC}(Ca(t))$ is the Ca^{2+}-dependent GC activity, $V_{GC}^{\max}$ is the maximum possible value of this activity, $Ca(t)$ is free cytoplasmic Ca2+, and ${}^{GC}K_{Ca}$ is the Ca^{2+} concentration at which the enzyme activity is half its maximum value. n_{GC} is a dimensionless parameter that denotes cooperativity.

Time course of light-dependent changes in cytoplasmic cGMP concentration

The light-dependent rate of cGMP hydrolysis is determined by PDE* catalytic activity, ${}^{light}V_{PDE}$, where:

$$ {}^{light}V_{PDE}(VP^*, cGMP) = \varepsilon_{sub} PDE^* \frac{cGMP(t)}{cGMP(t) + {}^{cGMP}K_m} \tag{2.12}$$

PDE* is the number of light-activated PDE molecules (the integral of equation (2.8)), *cGMP* is the nucleotide concentration, ${}^{cGMP}K_m$ is the PDE Michaelis-Menten constant for cGMP and

$$\varepsilon_{sub} = \frac{k_{cat}}{LV_{OS}} \tag{2.13}$$

k_{cat} (sec^{-1}) is the enzymatic turnover rate per PDE*. L is Avogadro's number and V_{OS} is the photoreceptor outer segment cytoplasmic volume (half the geometrical volume).

The rate at which a metabolite is produced (or destroyed) during a bioprocess is calculated from its metabolic flux ((Goldberg et al., 1983; Ames et al., 1986)). Metabolic flux is a flux balance analysis used to determine the rate at which a metabolite is. cGMP metabolic flux, the net rate of change of cGMP in the course of a light-elicited response is given by the difference between its rate of synthesis by GC and hydrolysis by PDE.

$$\frac{dcGMP(VP^*, Ca, cGMP)}{dt} = (V_{GC}(Ca(t)) - ({}^{dark}V_{PDE} + {}^{dark}V_{PDE}(VP^*, cGMP)) \tag{2.14}$$

cGMP-gated, Ca-modulated membrane current

The simultaneous changes in free Ca^{2+} (integral of text equation (2.10)) and cGMP concentrations (integral of text equation (2.14) are then used to compute the light-dependent changes in circulating outer segment current (equations (1.1) and (1.2)).

Flash photocurrent sensitivity and kinetics

Figure 1 illustrates changes in the circulating outer segment current caused by flash illumination of a dark adapted tiger salamander rod and a striped bass single cone. Currents were measured at room temperature under voltage clamp, by convention the holding current was defined as zero and the suppression of the inward current shown as an upward change (the photocurrent). The data in Figure 1 illustrate the archetypical differences in the transduction signal of dark-adapted rods and cones.

In both rods and cones, the peak amplitude of the signal is a function of intensity well described by an exponential saturation function (Lamb et al., 1981):

$$I(VP^*) = \mathrm{I}peak(1 - \exp(-VP^*/k)) \tag{2.15}$$

where *Ipeak* is the maximum value of the photocurrent peak amplitude, *VP** is light intensity expressed as the number of excited VP molecules in the cell and k is an adjustable parameter ($\sigma = \ln 2k$ is the light intensity at which current amplitude is half its maximum value). Mean *Ipeak* and σ values for salamander rods and bass cones are listed in Table 2. The light response is faster in cones than rods, made evident by the shorter time to the photocurrent peak amplitude (Table 2).

Optimized fit of model simulations to experimental data

The mathematical model of the phototransduction pathway can simulate photocurrents, but such exercise is useful only to the extent that values of the many parameters in the model are not all freely adjusted, but constrained by known biochemical and biophysical facts. Such constraints make matching simulated and experimental data less capricious, and validate using the model as a quantitative tool to evaluate the significance of known rod cone differences. The model, however, should be taken as a work in progress and not complete; it is a shorthand representation of what we know now, but it cannot predict what may yet be discovered.

Selection of parametric values

To fit simulated to experimental data we divide model parameters into three categories: Invariant, Statistical, and Adjustable. “Invariant” parameters are selected from the available literature and their values are kept the same for all cells and all simulations. “Statistical” parameters are experimentally measured in each cell under analysis. “Adjustable” parameters are adjusted to optimize the fit between simulated and experimental currents in each cell under study. Adjustments were made with computer-assistance to fit simulated to experimental data by least square minimization (Raphson-Newton, tolerance=0.001). The values of adjustable parameters are not arbitrary; their initial values were constrained, whenever possible, by experimentally known values. Tables 3 and 4 list parametric values arrived at through simulations and footnotes cite the constraining experimental facts.

Simulations were particularly sensitive to the following adjustable parameters: 1) The features of the $Na^+/Ca^{2+}K^+$ exchanger transport, $I_{NCKX}^{\max}$ and K_{Ca}^{exc} (text equation (1.7)). They were constrained by demanding their value be the same in the dark and the light for the same cell, by their ability to match the known light-dependent changes in cytoplasmic free Ca^{2+} concentration (Gray-Keller et al., 1999; Sampath et al., 1999), as well as biochemical data on the ionic dependence of the exchanger function (Lagnado et al., 1992; Sheng et al., 2000). 2) The features of cytoplasmic Ca^{2+} buffers (text equation (1.8)). They were constrained by demanding their value be the same in the dark and the light and their initial values consistent with data available for Ca^{2+} buffering in rod outer segments (Lagnado et al., 1992). 3) The relative contributions of VP* phosphorylation γ (text equation (2.1)) and PDE inactivation rate α_{PDE} (text equation (2.8)) to the control of the time course of PDE* inactivation (text equation (2.8)).

Experimental and model-simulated flash photocurrents in dark-adapted rods and cones

Photocurrents elicited by light flashes of varying intensity in a dark-adapted bass single cone are illustrated in Figure 2. Shown are both experimental and simulated photocurrents optimally fit to the experimental data. Values of the model parameters used in the simulations are presented in Table 3, cone 1. The range of quality of fit between model and experimental data is shown in Figure 3, using 2 additional cones. Parametric values in these simulations are also presented in Table 3, cones 2 and 3.

Figures 4 and 5 illustrate experimental and simulated photocurrents elicited by flashes presented to 3 different dark-adapted tiger salamander rods. The parametric values used to compute the simulated photocurrents in the Figures are listed in Table 4. Table 5 presents side by side the mean ± SD of parametric values inferred from successful analytical simulations measured in 18 cones and 9 rods.

Simulated photocurrents fit experimental data well except for the small, nearly exponential component observed as photocurrent amplitude approaches its maximum (saturated) amplitude. This component is generated by the electrogenic activity of the $Na^+/Ca^{2+}K^+$ exchanger (Nakatani and Yau, 1989; Perry and McNaughton, 1991). Although simulations illustrated here do not explicitly display this component, it is an implicit constituent of all model simulations. The time course of this electrogenic current reflects the dynamics of the light-dependent change in free cytoplasmic Ca^{2+}, and is given (in pA) by $I_{NCKX}^{\max} Ca/Ca+K_{Ca}^{exc}$ (from equation (1.7)). Therefore, the accuracy of the model to simulate free Ca^{2+} dynamic is also reflected in the accuracy with which the computed NCKX electrogenic current fits experimental data. Figure 6 illustrates the electrogenic NCKX current measured in a bass single cone and the computed NCKX exchanger current. To emphasize, the model computations were fit to the photocurrents measured in this cone at various light intensities, not specifically to the NCKX current. The simulated NCKX current is simply one of the components of the phototransduction process. The quality of the fit between computed and experimental data is very good and attests to the strength of the model computations.

Side by side comparison of the molecular events in the phototransduction pathway of rods and cones

Successful photocurrent simulations constrained by experimental facts allow side-by-side comparison of the molecular events that underlie phototransduction in rods and cones, evaluation of the significance of their differences and similarities, and assessment of important information gaps. To compare and contrast the dynamics of various molecular events in rods and cones a sequence of figures illustrates computed functions that depict the time course and amplitude of several molecular events which contribute to the simulated photocurrents illustrated for cone 1 (Figure 2) and rod 1 (Figure 4). For the cone and rod, the signals illustrated were elicited by flashes of intensity near the σ value of each photoreceptor or just above the amplitude-saturating intensity.

Visual pigment activation and inactivation: VP kinase activity and the regulatory role of Recoverin and Arrestin

The rate of VP* activation in rods and cones is determined by the number and delivery rate of stimulus photons. The time constant of formation of VP* (Meta-II) is very nearly the same for rod and cone opsins regardless of the wavelength of their absorbance maximum (Imai et al., 1995; Imai et al., 1997; Vought et al., 1999; Kusnetzow et al., 2001). For example, at room temperature, it is about 10 ms in chicken green opsin (λmax 508 nm) and 30 ms in chicken rhodopsin (λmax 503 nm) (Imai et al., 1995). In contrast, the rate of Meta-II decay is much faster in cones than rods. In VP detergent solutions, for example, the time constant of disappearance is 7 s in chicken green opsin but 210 s in chicken rhodopsin (Imai et al., 1995). Thus, Meta-II lifetime can be expected to be much shorter in cones than rods. The kinetic differences measured in detergent solutions are not necessarily the same as the opsin photodynamics in intact membranes. In micro-spectrophotometric studies with intact goldfish cones and rods, however, hydrolysis of the linkage between opsin and the bleached chromophore (all-trans 3-dehydroretinal) at room temperature has a half-time of about 5 sec in cones and about two orders of magnitude slower in rods (Golobokova and Govardovskii, 2006). In both rods and cones, and for light levels that do not bleach a significant fraction of the VP, photochemical decay of MetaII is slow, much too slow to explain photocurrent recovery, and other mechanisms are responsible for the inactivation of the VP* state. Nevertheless, as we document below, the lifetime of the VP* “active state” is, indeed, much shorter in intact cones than in rods.

From simulations, the time constant of VP* inactivation at near σ light intensity was 0.8–1.2 sec in rods and 0.03–0.04 sec in cones. Experimental studies in truncated toad rods at comparable intensities measure this time constant to be 2–2.5 sec (Rieke and Baylor, 1998). This very large rod-cone difference is explained by the biochemical properties of the opsin kinase function in the two receptor types. Comparing data from fish rods and cones, VP*-kinase catalytic rate per molecule is higher in cones (~5 Pi on VP*/GRK sec) than rods (~0.5 Pi on VP*/GRK sec) and the enzyme concentrations are also 10-fold higher in cones than rods,~0.04 GRK/VP and ~ 0.004 GRK/VP respectively (Tachibanaki et al., 2005). Consistent with biochemical facts, model simulations show VP*-kinase catalytic velocity in bass cones is about 25 times larger than that in salamander rods (Tables 3, 4 and 5. Figure 7B).

In the process of inactivation, VP* is phosphorylated multiple times and the maximum VP-kinase activity increases as the cytoplasmic Ca^{2+} concentration declines. The Ca^{2+}-dependence of GRK activity in the simulations was assigned the features known from biochemical measurements in rods (Kawamura, 1999), comparable experimental data is unavailable for cones. Model simulations were successful under the assumption that the Ca^{2+} sensitivity of rod and cone VP*-kinase (mediated by Recoverin) is the same.

The number of VP* sites phosphorylated in the course of the photoresponse in intact rods or cones is controversial. Biochemical evidence indicates that up to 4 sites can be phosphorylated in intact fish cone opsin (Kennedy et al., 2004). We adopted 6 as the number of physiologically relevant phosphorylation sites because of recent compelling results in mice rods: the reproducibility of single photon responses in transgenic rods matches that of the wild type rod only when 6, and no less than 6, phosphorylation sites are available in the rhodopsin molecules (Doan et al., 2006). Theoretical simulations of the reproducibility of single photon responses in toad rods also match experimental data when rhodopsin is assumed to be phosphorylated at 6 different sites (Hamer et al., 2003), although theoretical exception has been expressed (Caruso et al., 2010).

The model assumes the rate of quenching of phosphorylated-VP* by Arrestin is the same in rods and cones. This assumption is consistent with biochemical investigations in fish retina which show that inhibitory effects of Arrestin on rod and cone GRK are indistinguishable (Arinobu et al., 2010).

Gain in Transducin activation

The gain rate between VP* and the activation of transducin is known from experiments in toad rods to be ~150 T*/VP*sec (Leskov et al., 2000). This was the initial value assigned in the rod photocurrent simulations (Tables 4 and 5). The same parameter has not been experimentally measured in cones, but the T*/VP* rate gain arrived at through the successful cone simulations was a few-fold larger in cones than rods (Tables 3 and 5). The initial rate of rise of the photocurrent continues to increase with light intensity well after photocurrent amplitude is saturated and it reaches a maximum value only when a significant fraction of the VP is bleached (Cobbs and Pugh, 1987; Hestrin and Korenbrot, 1990). In the limit of bright light stimuli, when the initial rate of rise is near its maximum value, the value of this maximum initial rate of rise reflects the rate of PDE* activation (Cobbs and Pugh, 1987). Experimentally, the initial rate of rise of the photocurrent activated by flashes that bleach several percent of the VP are indistinguishable in cones from rods (Cobbs and Pugh, 1987; Hestrin and Korenbrot, 1990), consistent with the conclusion that the maximum stoichiometric rates of T* and PDE* activation are similar in the two photoreceptor types.

The electrophysiological and simulation studies may also help understand the mechanisms behind the finding that replacing rod transducin with cone transducin lowers the

photosensitivity of transgenic mice rods mice when compared with wild type (Chen et al., 2010a). The loss in the gain between light intensity and photocurrent amplitude is unlikely to reflect a difference in the VP* to T* gain rate. More likely, lifetime of the T* state of cone transducin is shorter than that of rod transducin in the mouse rod because of differences in the interactions between T* and the "RGS9" protein complex that inactivates T* (Wensel, 2008; Burns and Pugh, 2010).

The efficiency of T* activation by VP* decreases exponentially with the number of phosphorylated sites; experiments show that activation efficiency of transducin by rhodopsin declines by half with every added Pi in rods (Gibson et al., 2000). The relationship between T* activation and the state of VP*phosphorylation is unknown for cones, but simulations were successful under the assumption that it is the same as in rods (Tables 3, 4 and 5).

PDE* activation and inactivation

A particularly informative illustration of the differences in the phototransduction pathway of rods and cones is presented in Figure 8. Shown are simulations of the light-dependent changes in PDE and GC enzymatic activities in rods and cones at dim and bright light stimulation. The principal output of the transduction cascade, an initial decrease in cGMP concentration and its subsequent recovery, arises from the imbalance in the activities of the two enzymes. Initially PDE velocity exceeds that of GC and then GC exceeds the PDE velocity. The changes in enzyme activity are extremely stable and reproducible, and the dynamics of these changes define the waveform and sensitivity of the cGMP concentration change and, therefore, the waveform and light-dependence of the photocurrent. The rate of PDE* inactivation is much faster in cones than rods (Figure 8) (Tables 3 and 4).

The inactivation of PDE* reflects two sequential, but distinct processes: 1) inactivation of VP* by phosphorylation and 2) disappearance of T*. But, what are the dynamics of the contribution of the two reactions to the overall control of PDE* inactivation? This question can be answered with some confidence only with respect to photocurrents elicited by bright flashes, those that saturate the photocurrent amplitude. Pepperberg et al ((Pepperberg et al., 1992) proposed that under these conditions, one and only one biochemical reaction is the slowest one and its rate dominates the rate of PDE* inactivation. Electrophysiological experiments in salamander rods show that the dominant rate constant in the amplitude-saturated light response is Ca^{2+}-independent and, therefore, it was identified as the rate of T* disappearance (Nikonov et al., 1998). In contrast, experiments in tiger salamander cones find the dominant rate constant that controls the duration of amplitude-saturated photocurrents is Ca^{2+}-dependent and, therefore, the rate of VP* phosphorylation was identified as the rate-limiting reaction (Matthews and Sampath, 2010). Indeed, rod photocurrent simulations were successful under the assignment that T* disappearance controlled the termination of the photocurrent (Figures 4 and 5). Also, in cones experimental amplitude-saturated photocurrents could be fit only by adjusting the rate of VP* phosphorylation (Figures 2 and 3) (Korenbrot, 2012).

Photocurrent recovery at less than amplitude saturating intensities is complex because it is not controlled by a single, dominant rate constant. In fact, in rods it is not controlled by the inactivation of PDE* alone, but by a combination of the rate of PDE* inactivation and GC activation by the changing cytoplasmic Ca^{2+}. Simulations such as those in Figure 8 visualize the plausible contribution of the various biochemical reactions. Recent work in intact frog rods suggests that when light-dependent Ca^{2+} concentration changes are prevented, the kinetics of the recorded dim light photocurrent cannot be unambiguously attributed to either VP* phosphorylation or T* disappearance and both contribute to the control of the photocurrent time course (Astakhova et al., 2008). However, there is a difference between rods and cones. In cones, experimental and modeling considerations suggest the kinetics of

photocurrent recovery, even at low light intensities, are dominated by the dynamics of PDE* inactivation and not GC activation by Ca^{2+} (Hamer and Tyler, 1995; Korenbrot and Rebrik, 2002). Indeed, at intensities that do not saturate photocurrent amplitude, good fits between simulated and experimental data in cones can only be obtained by assigning T* disappearance as the dominant rate constant (Korenbrot, 2012) (Figure 8).

Another important difference between rods and cones is apparent in the features of their response light that bleaches a significant fraction of the VP, a condition not investigated in the present analysis. At pigment bleaching-light levels, rods saturate and cease to respond to light. In cones, in contrast, even if light bleaches over 90% of the VP the resulting photocurrent will be at saturating amplitude for several seconds, but, nonetheless it will terminate with CNG channels reopening and the circulating outer segment current returning to its dark value (Estevez et al., 2006). Photocurrent recovery from saturation, just as with much dimmer lights, reflects inactivation of PDE*. However, at light levels that bleach a large percentage of VP* (above ~25%) PDE* inactivation is not rate limited by enzymatic processes (neither VP* phosphorylation nor T* disappearance), but by the thermal decay of the MetaII photoproduct. MetaII decay culminates in the separation of the all-trans chromophore from the cone opsin protein. Once MetaII decays, PDE is restored to its dark state and the cone will respond to light that excites the remaining 10 % dark VP, but, of course, with much, much less photosensitivity (Estevez et al., 2006).

The functional role of the rate of T* disappearance on the time course of rod photocurrents has been explored in studies of the consequence of overexpressing RGS9 in transgenic mice. Experimentally it was found that overexpression of RGS9, but not of GRK, accelerates photoresponse recovery (Krispel et al., 2006). These results affirm that in rods and at all intensities T* disappearance is slower than VP* phosphorylation and is the dominant rate constant. Further investigation has also shown that the turn-off rate of the rod photocurrent accelerates as RGS9 concentration increases (Burns and Pugh, 2009). These experimental findings have been explained by a conceptual model that posits T* and PDE* form a complex, T*/PDE*, that interacts with a second complex formed by the assembly of regulatory proteins RGS9, R9AP and Gβ5L and referred to simply as “RGS9”. According to this model, “RGS9” catalyzes the conversion of the T*/PDE* complex to inactive PDE with Michaelis-Menten kinetics (reviewed in (Burns and Pugh, 2010). Because of the Michaelis-Menten kinetic behavior, then, the velocity of conversion of T*/PDE* to inactive PDE conversion (and T* disappearance) is determined by the product of “RGS9” concentration and its catalytic activity (its k_{cat}/K_m value), thus explaining the observed dependence of photocurrent turn-off kinetics on RGS9 concentration.

The Burns-Pugh (2009) model offer an insightful explanation for the observed fact that PDE* inactivation is much quicker in cones than rods (Figure 8) (Tables 3, 4 and 5). The same RGS9 molecule is expressed in rods and cones, but its concentration is much higher in cones than rods (RGS9 to VP mole ratio is ~1:62 in cones and ~1:610 in rods) (Zhang et al., 2003). Hence, the difference in PDE* inactivation rate, between rods and cones can be explained by their difference in RGS9 concentration and can be expected to be about 10 times faster in cones than rods, just as inferred from the simulations (Table 5).

Rods and cones differ not only in the molecular mechanism underlying PDE inactivation, but also in the light-sensitivity of the inactivation reactions. As inferred from model simulations, α_{PDE} and γ_{max} in rods are essentially light independent over all intensities tested (Figure 9). In cones, however, both parameters are expected to be light dependent over the intensity range tested (Figure 9).

Calcium-dependent GC activity

In simulations, GC catalytic activity was assigned similar Ca^{2+}-dependence in rods and cones taken from data in the rod biochemical literature (Lolley and Racz, 1982; Koch and Stryer, 1988) because comparable data is not available for cones. On the other hand, Vmax was inferred from the simulations. However, there was little freedom in this adjustment: it was constrained both by the fact that total enzymatic activity in the dark was known and by the requirement that the Vmax applied in dark and light. The values arrived at indicate the maximum GC activity in cones is about 5-fold higher than in rods. Moreover the absolute mean values of GC Vmax (Table 5) are similar to those measured in truncated carp rods and cone outer segments (Takemoto et al., 2009).

Time course of light-dependent changes in cytoplasmic free Ca^{2+}

Figure 9 illustrates the simulated changes in free Ca^{2+} underlying the photocurrents of rod 1 and cone 1. The data are selected to compare Ca^{2+} changes at intensities that cause approximately the same fractional change in membrane current, when the peak photocurrent is about half the saturating photocurrent amplitude and at intensities that just saturate photocurrent amplitude. The Ca^{2+} changes are much faster in cones than in rods, as has been long recognized (Korenbrot and Rebrik, 2002). At saturation, Ca^{2+} reaches its lowest concentration in about 1.2 sec in rods, but only 0.13 sec in cones. Ca^{2+} recovers with an approximately exponential time course of 2.7 sec time constant in rods, but only 0.45 sec in cones. In addition, for the same proportional change in current, Ca^{2+} is reduced by nearly 20% in rods, but about 70% in cones. The simulated light-dependent changes in outer segment free Ca^{2+} are similar to those measured experimentally (in rods (Gray-Keller and Detwiler, 1994; Younger et al., 1996); in cones: (Sampath et al., 1999; Leung et al., 2007).

Differences in the kinetics of light-dependent Ca^{2+} concentration changes between rods and cones arise from differences in each of the molecular processes that control outer segment free Ca^{2+}. The Ca^{2+} permeability is higher in cone than rod channels (Picones and Korenbrot, 1995; Dzeja et al., 1999), and at the same membrane current about twice as many Ca^{2+} ions enter the cone as the rod outer segment (Ohyama et al., 2000; Ohyama et al., 2002) (Table 5). Ca^{2+} efflux rate, the dominant component of the Ca^{2+} recovery at the end of the photoresponse is much slower in rods than cones. To fit simulated to experimental data in rods, we defined the Ca^{2+} -dependence of the $Na^{+}/Ca^{2+},K^{+}$ exchanger, K_{Ca}^{exc} (text equation (1.7)), to be invariant and with a value 1.6 μM based on experimental fact (Lagnado et al., 1992). However, when the same value was assigned in cone simulations, it was impossible to fit experimental data: the rate of Ca^{2+} efflux was much too slow. Successful fits were obtained only by assigning this variable a much lower value (Tables 3, 5), which yields a much higher Ca^{2+} transport rate at physiological free Ca^{2+} concentrations. This is contrary to the reported finding that the ionic-dependence of recombinant cone and rod exchangers are similar to each other (Sheng et al., 2000). However, it must be remembered that there are several splice variants of the exchanger molecule in bass cones (Paillart et al., 2007) and in the intact cell the exchanger forms a tight complex with the CNG channels (Bauer, 2002; Kang et al., 2003). It is possible the exchanger in an intact photoreceptor has different functional properties than the cloned exchanger. There is also the remarkable report than cones in transgenic mice that do not express the canonical NCKX2 exchanger appear to function normally, at least as evaluated with the electroretinogram (Li et al., 2006). The functional characteristics of the NCKX exchanger in an intact cone need to be characterized, much as they have been in rods (Lagnado et al., 1992).

Ca^{2+} buffer

Based on experimental findings in rods simulations assume both rods and cones have two cytoplasmic buffer systems one of high and one of low affinity (Lagnado et al., 1992). Initial values of buffer concentration and affinity were based on the available experimental data (Lagnado et al., 1992). The buffers capacity and dissociation constant inferred from the simulations were calculated through computer-aided fit of simulated to experimental data. Ca^{2+} buffer capacity may well be different in the two receptor types: the affinity constant of the low affinity buffer is not that different in rods and cones, but its concentration is 2- to 4-fold higher in cones than rods. In addition, the buffer capacity of the low affinity buffer is higher in cones than rods (Tables 2, 3, 4). The accuracy of these values is difficult to ascertain because experimental characterization of the buffers exists only for tiger salamander rods and it was conducted with what is by now a technically limited tool surpassed in current technology. This information void needs to be filled.

Ca-dependent modulation of CNG channel ligand sensitivity

The probability of CNG channels being open is controlled by cGMP, but modulated by Ca^{2+}. The cGMP sensitivity of channel activity is higher at low Ca^{2+} concentrations. Because of quantitative differences in the extent and Ca^{2+}-dependence of this modulation, in intact photoreceptors, cGMP alone controls CNG channel activity in rods, but in cones it is controlled by both cGMP and Ca^{2+}. Simulations shown in Figure 11 illustrate the physiological importance of this difference. As we expect, in the normal cone 1 and rod 1 a flash near σ intensity causes a decrease in cGMP, a decrease in cytoplasmic free Ca^{2+} Ca^{2+} and a reduction in the inward outer segment current. These changes are stable and reproducible. When Ca^{2+} control of channel activity is removed in the simulations (a computational knock out), there is little consequence in the rod response (Figure 11B). In stark contrast, when Ca^{2+} control of channel activity is removed in the cone every component of the photoresponse is affected and the photocurrent is larger and unstable. If Ca^{2+} modulation were not present, the responses in cones would be more sensitive, slower and would oscillate as they return to their dark state (additional details in (Korenbrot, 2012). Recent experiments in transgenic mice rods indeed affirm that obstructing the Ca-dependent CNG channel modulation is of little, if any, functional consequence (Chen et al., 2010b).

Conclusions and future directions

The molecular scheme of the phototransduction pathway is essentially the same in rods and cones, but the quantitative details of the function of each of the biochemical and biophysical processes in this pathway differ in the two receptor types. A mathematical representation of the currently accepted phototransduction pathway, constrained whenever possible by experimental values measured in biochemical assays or in the intact photoreceptor, proved remarkably successful in simulating experimental photocurrents. The model allowed side by side comparison of the dynamics of the molecular events of phototransduction in rods and cones. However, the model is simply a convenient tool to assemble and compare data available to date and to point out gaps in our information. Just as other models before, it would be reasonable to expect that the information will be improved and details of the model superseded as newer and better data becomes available.

It is remarkable that evolutionary pressures have succeeded in yielding such different end point-performance from transduction pathways qualitatively so very similar. Examination of Figures 7, 8, 9, and the Tables demonstrate evolutionary success reflects several different strategic choices: 1) genomically-related proteins perform similar functions but with very different quantitative features (GRK for example). 2) proteins of near identical function are

expressed at different concentration (RGS9 for example). 3) proteins of similar structure and function are under very different regulation (CNG channels for example).

Cytoplasmic Ca^{2+} acts as a powerful feedback regulator in both rods and cones. Just as in all other cells where Ca^{2+} acts as a second messenger, cytoplasmic buffers are critical in defining the spatial and temporal features of the Ca^{2+} signal. The properties and identity of these buffers, however, are only known for rods and not at all for cones. Future experimental work must address this serious shortcoming, especially in view of the availability of new tools to carry out this task.

Phototransduction occurs even in the absence of light-dependent changes in cytoplasmic Ca^{2+} in both rods and cones, but the functional features of such signals are far different from those measured under normal conditions (Nakatani and Yau, 1988; Fain et al., 1989; Matthews et al., 1990). What is gained by Ca-dependent controls is not the difference between transduction and the failure to transduce, but the ability to regulate the molecular events underlying phototransduction. The regulatory function of Ca^{2+} in phototransduction is a feedback control mechanism because the output of phototransduction, a decrease in cytoplasmic Ca^{2+}, influences the events that lead to the change in Ca^{2+} in the first place. It is a negative feedback because the output is fed back in such a way as to partially oppose the input. Signal stability is a serious challenge in the design of engineering systems that are controlled through negative feedback. The simulations show that Ca^{2+}-feedback signals are stable in rods when CNG channel activity is controlled by cGMP alone. Control of channel activity by both cGMP and Ca^{2+} has evolved to attain well-controlled and stable photoresponses that meet the imperatives of time course, sensitivity, and light adaptation that sustain the cone transduction function, far different as they are from the rod transduction function.

We reviewed in detail the response of the phototransduction pathway to flash stimuli, a convenient experimental paradigm, but rarely a condition in typical visually driven behavior. The response to steps of light and to flashes superimposed on steps of varying intensity (light adaptation), of course, depend on the same mechanisms as the flash response, but additional changes in the dynamics of some of the molecules of the transduction pathway must also be invoked. It is clear that Ca^{2+} plays an important role in light adaptation, but other molecular processes have also been identified, for example, changes in PDE* lifetime (in rods (Nikonov et al., 2000), in cones (Soo et al., 2008); (Korenbrot, 2012a) and modulation of the ligand sensitivity of the CNG channels in cones (Rebrik et al., 2012b). Future research needs to discover all the molecular events of light adaptation in the detail in which it is now possible to describe the dark-adapted response. When these details are fully resolved, however, the general message will likely be the same as can be said of the differences in the dark adapted response. Physiological differences between any two cells, rods from cones or cones subtypes from each other, do not arise from the function of any one protein alone or any one regulatory process alone, but from aggregated changes in the system of reactions that constitute the transduction pathway as a whole.

References

Alvarez O, Gonzalez C, Latorre R. Counting channels: a tutorial guide on ion channel fluctuation analysis. Adv Physiol Educ. 2002; 26:327–341. [PubMed: 12444005]

Ames A 3rd, Walseth TF, Heyman RA, Barad M, Graeff RM, Goldberg ND. Light-induced increases in cGMP metabolic flux correspond with electrical responses of photoreceptors. J Biol Chem. 1986; 261:13034–13042. [PubMed: 2875993]

Ames JB, Levay K, Wingard JN, Lusin JD, Slepak VZ. Structural basis for calcium-induced inhibition of rhodopsin kinase by recoverin. J Biol Chem. 2006; 281:37237–37245. [PubMed: 17020884]

Arendt D. Evolution of eyes and photoreceptor cell types. Int J Dev Biol. 2003; 47:563–571. [PubMed: 14756332]

Arinobu D, Tachibanaki S, Kawamura S. Larger inhibition of visual pigment kinase in cones than in rods. J Neurochem. 2010; 115:259–268. [PubMed: 20649847]

Astakhova LA, Firsov ML, Govardovskii VI. Kinetics of turn-offs of frog rod phototransduction cascade. J Gen Physiol. 2008; 132:587–604. [PubMed: 18955597]

Bader CR, Bertrand D, Schwartz EA. Voltage-activated and calcium-activated currents studied in solitary rod inner segments from the salamander retina. J Physiol. 1982; 331:253–284. [PubMed: 7153904]

Bargmann, CI. WormBook. 2006. Chemosensation in C. elegans; p. 1-29.

Barnes S, Hille B. Ionic channels of the inner segment of tiger salamander cone photoreceptors. J Gen Physiol. 1989; 94:719–743. [PubMed: 2482325]

Bauer PJ. Cyclic GMP-gated channels of bovine rod photoreceptors: affinity, density and stoichiometry of Ca2+-calmodulin binding sites. J Physiol. 1996; 494:675–685. [PubMed: 8865065]

Bauer PJ. The complex of cGMP-gated channel and Na+/Ca2+, K+ exchanger in rod photoreceptors. Adv Exp Med Biol. 2002; 514:253–274. [PubMed: 12596926]

Baylor DA, Fuortes MG. Electrical responses of single cones in the retina of the turtle. J Physiol. 1970; 207:77– 92. [PubMed: 4100807]

Baylor DA, Hodgkin AL. Detection and resolution of visual stimuli by turtle photoreceptors. J Physiol. 1973; 234:163–198. [PubMed: 4766219]

Baylor DA, Lamb TD, Yau KW. The membrane current of single rod outer segments. J Physiol. 1979a; 288:589–611. [PubMed: 112242]

Baylor DA, Lamb TD, Yau KW. Responses of retinal rods to single photons. J Physiol. 1979b; 288:613–634. [PubMed: 112243]

Baylor DA, Matthews G, Yau KW. Two components of electrical dark noise in toad retinal rod outer segments. J Physiol. 1980; 309:591–621. [PubMed: 6788941]

Baylor DA, Matthews G, Yau KW. Temperature effects on the membrane current of retinal rods of the toad. J Physiol. 1983; 337:723–734. [PubMed: 6410058]

Baylor DA, Nunn BJ, Schnapf JL. The photocurrent, noise and spectral sensitivity of rods of the monkey macaca fascicularis. J Physiol. 1984; 357:575–607. [PubMed: 6512705]

Baylor DA, Nunn BJ. Electrical properties of the light-sensitive conductance of rods of the salamander Ambystoma tigrinum. J Physiol. 1986; 371:115–145. [PubMed: 2422346]

Baylor DA, Burns ME. Control of rhodopsin activity in vision. Eye (London, England). 1998; 12 (Pt 3b):521–525.

Berlin JR, Bassani JW, Bers DM. Intrinsic cytosolic calcium buffering properties of single rat cardiac myocytes. Biophys J. 1994; 67:1775–1787. [PubMed: 7819510]

Biel M, Michalakis S. Cyclic nucleotide-gated channels. Handbook of experimental pharmacology. 2009:111–136. [PubMed: 19089328]

Blythe HI, Liversedge SP, Joseph HS, White SJ, Findlay JM, Rayner K. The binocular coordination of eye movements during reading in children and adults. Vision Res. 2006; 46:3898–3908. [PubMed: 16879851]

Borwein, B. The retinal receptors: a description. In: Enoch, JM.; Tobey, FL., editors. Vertebrate photoreceptor optics. Springer-Verlag; Berlin: 1981. p. 11-82.

Brown BM, Ramirez T, Rife L, Craft CM. Visual Arrestin 1 contributes to cone photoreceptor survival and light adaptation. Invest Ophthalmol Vis Sci. 2010; 51:2372–2380. [PubMed: 20019357]

Bucossi G, Nizzari M, Torre V. Single-channel properties of ionic channels gated by cyclic nucleotides. Biophys J. 1997; 72:1165–1181. [PubMed: 9138564]

Burkhardt DA, Gottesman J. Light adaptation and responses to contrast flashes in cones of the walleye retina. Vision Res. 1987; 27:1409–1420. [PubMed: 3445477]

Burkhardt DA. Light adaptation and photopigment bleaching in cone photoreceptors in situ in the retina of the turtle. J Neurosci. 1994; 14:1091–1105. [PubMed: 8120614]

Burns ME, Pugh EN Jr. RGS9 concentration matters in rod phototransduction. Biophys J. 2009; 97:1538–1547. [PubMed: 19751658]

Burns ME, Pugh EN Jr. Lessons from photoreceptors: turning off g-protein signaling in living cells. Physiology (Bethesda). 2010; 25:72–84. [PubMed: 20430952]

Cameron DA, Pugh EN Jr. The magnitude, time course and spatial distribution of current induced in salamander rods by cyclic guanine nucleotides. J Physiol. 1990; 430:419–439. [PubMed: 1964967]

Carleton KL, Spady TC, Cote RH. Rod and cone opsin families differ in spectral tuning domains but not signal transducing domains as judged by saturated evolutionary trace analysis. J Mol Evol. 2005; 61:75–89. [PubMed: 15988624]

Caruso G, Bisegna P, Lenoci L, Andreucci D, Gurevich VV, Hamm HE, DiBenedetto E. Kinetics of rhodopsin deactivation and its role in regulating recovery and reproducibility of rod photoresponse. PLoS Comput Biol. 2010; 6:e1001031. [PubMed: 21200415]

Cervetto L, Lagnado L, Perry RJ, Robinson DW, McNaughton PA. Extrusion of calcium from rod outer segments is driven by both sodium and potassium gradients. Nature. 1989; 337:740–743. [PubMed: 2537471]

Chen CK, Zhang K, Church-Kopish J, Huang W, Zhang H, Chen YJ, Frederick JM, Baehr W. Characterization of human GRK7 as a potential cone opsin kinase. Mol Vis. 2001; 7:305–13. [PubMed: 11754336]

Chen CK. The vertebrate phototransduction cascade: amplification and termination mechanisms. Rev Physiol Biochem Pharmacol. 2005; 154:101–21. [PubMed: 16634148]

Chen CK, Woodruff ML, Chen FS, Shim H, Cilluffo MC, Fain GL. Replacing the rod with the cone transducin subunit decreases sensitivity and accelerates response decay. J Physiol. 2010a; 588:3231–3241. [PubMed: 20603337]

Chen J, Makino CL, Peachey NS, Baylor DA, Simon MI. Mechanisms of rhodopsin inactivation in vivo as revealed by a COOH-terminal truncation mutant. Science. 1995; 267:374–377. [PubMed: 7824934]

Chen J, Woodruff ML, Wang T, Concepcion FA, Tranchina D, Fain GL. Channel modulation and the mechanism of light adaptation in mouse rods. J Neurosci. 2010b; 30:16232–16240. [PubMed: 21123569]

Choe HW, Kim YJ, Park JH, Morizumi T, Pai EF, Krauss N, Hofmann KP, Scheerer P, Ernst OP. Crystal structure of metarhodopsin II. Nature. 2011; 471:651–655. [PubMed: 21389988]

Cobbs WH, Pugh EN Jr. Kinetics and components of the flash photocurrent of isolated retinal rods of the larval salamander, Ambystoma tigrinum. J Physiol. 1987; 394:529–572. [PubMed: 2832596]

Colamartino G, Menini A, Torre V. Blockage and permeation of divalent cations through the cyclic gmpactivated channel from tiger salamander retinal rods. J Physiol. 1991; 440:189–206. [PubMed: 1725182]

Conti M, Beavo J. Biochemistry and physiology of cyclic nucleotide phosphodiesterases: essential components in cyclic nucleotide signaling. Annu Rev Biochem. 2007; 76:481–511. [PubMed: 17376027]

Cook NJ, Molday LL, Reid D, Kaupp UB, Molday RS. The cGMP-gated channel of bovine rod photoreceptors is localized exclusively in the plasma membrane. J Biol Chem. 1989; 264:6996–6999. [PubMed: 2468664]

Corey DP, Dubinsky JM, Schwartz EA. The calcium current in inner segments of rods from the salamander (Ambystoma tigrinum) retina. J Physiol. 1984; 354:557–575. [PubMed: 6090654]

D'Amours MR, Cote RH. Regulation of photoreceptor phosphodiesterase catalysis by its non-catalytic cGMP-binding sites. Biochem J. 1999; 340 (Pt 3):863–869. [PubMed: 10359674]

Davies WL, Hankins MW, Foster RG. Vertebrate ancient opsin and melanopsin: divergent irradiance detectors. Photochemical & photobiological sciences: Official journal of the European Photochemistry Association and the European Society for Photobiology. 2010; 9:1444–1457.

Dizhoor AM, Lowe DG, Olshevskaya EV, Laura RP, Hurley JB. The human photoreceptor membrane guanylyl cyclase, RetGC, is present in outer segments and is regulated by calcium and a soluble activator. Neuron. 1994; 12:1345–1352. [PubMed: 7912093]

Dizhoor AM, Olshevskaya EV, Henzel WJ, Wong SC, Stults JT, Ankoudinova I, Hurley JB. Cloning, sequencing, and expression of a 24-kDa Ca(2+)-binding protein activating photoreceptor guanylyl cyclase. J Biol Chem. 1995; 270:25200–25206. [PubMed: 7559656]

Dizhoor AM, Hurley JB. Regulation of photoreceptor membrane guanylyl cyclases by guanylyl cyclase activator proteins. Methods. 1999; 19:521–531. [PubMed: 10581151]

Dizhoor AM, Olshevskaya EV, Peshenko IV. Mg2+/Ca2+ cation binding cycle of guanylyl cyclase activating proteins (GCAPs): role in regulation of photoreceptor guanylyl cyclase. Mol Cell Biochem. 2010; 334:117–124. [PubMed: 19953307]

Doan T, Mendez A, Detwiler PB, Chen J, Rieke F. Multiple phosphorylation sites confer reproducibility of the rod's single-photon responses. Science. 2006; 313:530–533. [PubMed: 16873665]

Downs MA, Arimoto R, Marshall GR, Kisselev OG. G-protein alpha and beta-gamma subunits interact with conformationally distinct signaling states of rhodopsin. Vision Res. 2006; 46:4442–4448. [PubMed: 16989885]

Dumke CL, Arshavsky VY, Calvert PD, Bownds MD, Pugh EN Jr. Rod outer segment structure influences the apparent kinetic parameters of cyclic GMP phosphodiesterase. J Gen Physiol. 1994a; 103:1071–1098. [PubMed: 7931138]

Dumke CL, Arshavsky VY, Calvert PD, Bownds MD, Pugh EN Jr. Rod outer segment structure influences the apparent kinetic parameters of cyclic GMP phosphodiesterase. J Gen Physiol. 1994b; 103:1071–1098. [PubMed: 7931138]

Dzeja C, Hagen V, Kaupp UB, Frings S. Ca2+ permeation in cyclic nucleotide-gated channels. EMBO J. 1999; 18:131–144. [PubMed: 9878057]

Eismann E, Muller F, Heinemann SH, Kaupp UB. A single negative charge within the pore region of a cGMP-gated channel controls rectification, Ca2+ blockage, and ionic selectivity. Proc Natl Acad Sci U S A. 1994; 91:1109–1113. [PubMed: 7508120]

Estevez ME, Ala-Laurila P, Crouch RK, Cornwall MC. Turning cones off: the role of the 9-methyl group of retinal in red cones. J Gen Physiol. 2006; 128:671–685. [PubMed: 17101818]

Fain GL, Lamb TD, Matthews HR, Murphy RL. Cytoplasmic calcium as the messenger for light adaptation in salamander rods. J Physiol. 1989; 416:215–243. [PubMed: 2607449]

Fain GL, Hardie R, Laughlin SB. Phototransduction and the evolution of photoreceptors. Curr Biol. 2010; 20:R114–124. [PubMed: 20144772]

Fesenko EE, Kolesnikov SS, Lyubarski AL. Induction by cyclic GMP of cationic conductance in plasma membrane of retinal rod outer segments. Nature. 1985; 313:310–313. [PubMed: 2578616]

Fetter RD, Corless JM. Morphological components associated with frog cone outer segment disc margins. Invest Ophthalmol Vis Sci. 1987; 28:646–657. [PubMed: 3493999]

Flaherty KM, Zozulya S, Stryer L, McKay DB. Three-dimensional structure of recoverin, a calcium sensor in vision. Cell. 1993; 75:709–716. [PubMed: 8242744]

Forti S, Menini A, Rispoli G, Torre V. Kinetics of phototransduction in retinal rods of the newt Triturus cristatus. J Physiol. 1989; 419:265–295. [PubMed: 2621632]

Fredriksson R, Lagerstrom MC, Lundin LG, Schioth HB. The G-protein-coupled receptors in the human genome form five main families. Phylogenetic analysis, paralogon groups, and fingerprints. Mol Pharmacol. 2003; 63:1256–1272. [PubMed: 12761335]

Frings S, Seifert R, Godde M, Kaupp UB. Profoundly different calcium permeation and blockage determine the specific function of distinct cyclic nucleotide-gated channels. Neuron. 1995; 15:169–179. [PubMed: 7542461]

Fu Y, Yau KW. Phototransduction in mouse rods and cones. Pflugers Arch. 2007; 454:805–819. Epub 2007 Jan 2017. [PubMed: 17226052]

Gibson SK, Parkes JH, Liebman PA. Phosphorylation modulates the affinity of light-activated rhodopsin for G protein and arrestin. Biochemistry. 2000; 39:5738–5749. [PubMed: 10801324]

Gillespie PG, Beavo JA. Characterization of a bovine cone photoreceptor phosphodiesterase purified by cyclic GMP-sepharose chromatography. J Biol Chem. 1988; 263:8133–8141. [PubMed: 2836413]

Goldberg ND, Ames AA 3rd, Gander JE, Walseth TF. Magnitude of increase in retinal cGMP metabolic flux determined by 18O incorporation into nucleotide alpha-phosphoryls corresponds with intensity of photic stimulation. J Biol Chem. 1983; 258:9213–9219. [PubMed: 6307996]

Golobokova EY, Govardovskii VI. Late stages of visual pigment photolysis in situ: cones vs. rods. Vision Res. 2006; 46:2287–2297. [PubMed: 16473387]

Gorczyca WA, Polans AS, Surgucheva IG, Subbaraya I, Baehr W, Palczewski K. Guanylyl cyclase activating protein. A calcium-sensitive regulator of phototransduction. J Biol Chem. 1995; 270:22029–22036. [PubMed: 7665624]

Gordon SE, Downing-Park J, Zimmerman AL. Modulation of the cGMP-gated ion channel in frog rods by calmodulin and an endogenous inhibitory factor. J Physiol. 1995; 486:533–546. [PubMed: 7473217]

Gorodovikova EN, Gimelbrant AA, Senin II, Philippov PP. Recoverin mediates the calcium effect upon rhodopsin phosphorylation and cGMP hydrolysis in bovine retina rod cells. FEBS Lett. 1994; 349:187–190. [PubMed: 8050563]

Grant JE, Guo LW, Vestling MM, Martemyanov KA, Arshavsky VY, Ruoho AE. The N terminus of GTP gamma S-activated transducin alpha-subunit interacts with the C terminus of the cGMP phosphodiesterase gamma-subunit. J Biol Chem. 2006; 281:6194–6202. [PubMed: 16407279]

Gray-Keller M, Denk W, Shraiman B, Detwiler PB. Longitudinal spread of second messenger signals in isolated rod outer segments of lizards. J Physiol. 1999; 519:679–692. [PubMed: 10457083]

Gray-Keller MP, Detwiler PB. The calcium feedback signal in the phototransduction cascade of vertebrate rods. Neuron. 1994; 13:849–861. [PubMed: 7524559]

Gross OP, Burns ME. Control of rhodopsin's active lifetime by arrestin-1 expression in mammalian rods. J Neurosci. 2010; 30:3450–3457. [PubMed: 20203204]

Gurevich VV, Hanson SM, Song X, Vishnivetskiy SA, Gurevich EV. The functional cycle of visual arrestins in photoreceptor cells. Prog Retin Eye Res. 2011; 30:405–430. [PubMed: 21824527]

Hackos DH, Korenbrot JI. Calcium modulation of ligand affinity in the cyclic GMP-gated ion channels of cone photoreceptors. J Gen Physiol. 1997; 110:515–528. [PubMed: 9348324]

Hagins WA, Penn RD, Yoshikami S. Dark current and photocurrent in retinal rods. Biophys J. 1970; 10:380– 412. [PubMed: 5439318]

Hamer RD, Tyler CW. Phototransduction: modeling the primate cone flash response. Vis Neurosci. 1995; 12:1063–1082. [PubMed: 8962827]

Hamer RD. Computational analysis of vertebrate phototransduction: combined quantitative and qualitative modeling of dark- and light-adapted responses in amphibian rods. Vis Neurosci. 2000; 17:679–699. [PubMed: 11153649]

Hamer RD, Nicholas SC, Tranchina D, Liebman PA, Lamb TD. Multiple steps of phosphorylation of activated rhodopsin can account for the reproducibility of vertebrate rod single-photon responses. J Gen Physiol. 2003; 122:419–444. [PubMed: 12975449]

Hamer RD, Nicholas SC, Tranchina D, Lamb TD, Jarvinen JL. Toward a unified model of vertebrate rod phototransduction. Vis Neurosci. 2005; 22:417–436. [PubMed: 16212700]

Harosi FI, Novales Flamarique I. Functional significance of the taper of vertebrate cone photoreceptors. J Gen Physiol. 2012; 139:159–187. [PubMed: 22250013]

Haynes LW, Kay AR, Yau KW. Single cyclic GMP-activated channel activity in excised patches of rod outer segment membrane. Nature. 1986; 321:66–70. [PubMed: 2422558]

Haynes LW, Yau KW. Single channel measurement from the cGMP-activated conductance of catfish retinal cones. J Physiol. 1990; 429:451–481. [PubMed: 1703573]

Haynes LW. Permeation and block by internal and external divalent cations of the catfish cone photoreceptor cGMP-gated channel. J Gen Physiol. 1995; 106:507–523. [PubMed: 8786345]

Hemila S, Reuter T. Longitudinal spread of adaptation in the rods of the frog's retina. J Physiol. 1981; 310:501– 528. [PubMed: 6971931]

Hestrin S. The properties and function of inward rectification in rod photoreceptors of the tiger salamander. J Physiol. 1987; 390:319–333. [PubMed: 2450992]

Hestrin S, Korenbrot JI. Effects of cyclic GMP on the kinetics of the photocurrent in rods and in detached rod outer segments. J Gen Physiol. 1987; 90:527–551. [PubMed: 2824661]

Hestrin S, Korenbrot JI. Activation kinetics of retinal cones and rods: response to intense flashes of light. J Neurosci. 1990; 10:1967–1973. [PubMed: 2355261]

Hisatomi O, Matsuda S, Satoh T, Kotaka S, Imanishi Y, Tokunaga F. A novel subtype of G-proteincoupled receptor kinase, GRK7, in teleost cone photoreceptors. FEBS Lett. 1998; 424:159–164. [PubMed: 9539142]

Hisatomi O, Honkawa H, Imanishi Y, Satoh T, Tokunaga F. Three kinds of guanylate cyclase expressed in medaka photoreceptor cells in both retina and pineal organ. Biochem Biophys Res Comm. 1999; 255:216–220. [PubMed: 10049688]

Hodgkin AL, Nunn BJ. Control of light-sensitive current in salamander rods. J Physiol. 1988; 403:439–471. [PubMed: 2473195]

Holcman D, Korenbrot JI. Longitudinal diffusion in retinal rod and cone outer segment cytoplasm: the consequence of cell structure. Biophys J. 2004; 86:2566–2582. [PubMed: 15041693]

Holcman D, Korenbrot JI. The limit of photoreceptor sensitivity: molecular mechanisms of dark noise in retinal cones. J Gen Physiol. 2005; 125:641–660. [PubMed: 15928405]

Horn R, Marty A. Muscarinic activation of ionic currents measured by a new whole-cell recording method. J Gen Physiol. 1988; 92:145–159. [PubMed: 2459299]

Hsu YT, Molday RS. Interaction of calmodulin with the cyclic GMP-gated channel of rod photoreceptor cells. Modulation of activity, affinity purification, and localization. J Biol Chem. 1994; 269:29765–29770. [PubMed: 7525588]

Hu G, Wensel TG. R9AP, a membrane anchor for the photoreceptor GTPase accelerating protein, RGS9-1. Proc Natl Acad Sci U S A. 2002; 99:9755–9760. [PubMed: 12119397]

Huang D, Hinds TR, Martinez SE, Doneanu C, Beavo JA. Molecular determinants of cGMP binding to chicken cone photoreceptor phosphodiesterase. J Biol Chem. 2004; 279:48143–48151. [PubMed: 15331594]

Hurley JB, Spencer M, Niemi GA. Rhodopsin phosphorylation and its role in photoreceptor function. Vision Res. 1998; 38:1341–1352. [PubMed: 9667002]

Imai H, Imamoto Y, Yoshizawa T, Shichida Y. Difference in molecular properties between chicken green and rhodopsin as related to the functional difference between cone and rod photoreceptor cells. Biochemistry. 1995; 34:10525–10531. [PubMed: 7654707]

Imai H, Terakita A, Tachibanaki S, Imamoto Y, Yoshizawa T, Shichida Y. Photochemical and biochemical properties of chicken blue-sensitive cone visual pigment. Biochemistry. 1997; 36:12773–12779. [PubMed: 9335534]

Imanishi Y, Li N, Sokal I, Sowa ME, Lichtarge O, Wensel TG, Saperstein DA, Baehr W, Palczewski K. Characterization of retinal guanylate cyclase-activating protein 3 (GCAP3) from zebrafish to man. Eur J Neurosci. 2002; 15:63–78. [PubMed: 11860507]

Insinna C, Besharse JC. Intraflagellar transport and the sensory outer segment of vertebrate photoreceptors. Dev Dyn. 2008; 237:1982–1992. [PubMed: 18489002]

Jastrzebska B, Tsybovsky Y, Palczewski K. Complexes between photoactivated rhodopsin and transducin: progress and questions. Biochem J. 2010; 428:1–10. [PubMed: 20423327]

Johnson JL, Leroux MR. cAMP and cGMP signaling: sensory systems with prokaryotic roots adopted by eukaryotic cilia. Trends Cell Biol. 2010; 20:435–444. [PubMed: 20541938]

Jones GJ, Fein A, MacNichol EF Jr, Cornwall MC. Visual pigment bleaching in isolated salamander retinal cones. Microspectrophotometry and light adaptation. J Gen Physiol. 1993; 102:483–502. [PubMed: 8245820]

Kang K, Bauer PJ, Kinjo TG, Szerencsei RT, Bonigk W, Winkfein RJ, Schnetkamp PP. Assembly of retinal rod or cone Na(+)/Ca(2+)-K(+) exchanger oligomers with cGMP-gated channel subunits as probed with heterologously expressed cDNAs. Biochemistry. 2003; 42:4593–4600. [PubMed: 12693957]

Karpen JW, Loney DA, Baylor DA. Cyclic GMP-activated channels of salamander retinal rods: spatial distribution and variation of responsiveness. J Physiol. 1992; 448:257–274. [PubMed: 1375637]

Kaupp UB, Seifert R. Cyclic nucleotide-gated ion channels. Physiol Rev. 2002; 82:769–824. [PubMed: 12087135]

Kawamura S, Kuwata O, Yamada M, Matsuda S, Hisatomi O, Tokunaga F. Photoreceptor protein s26, a cone homologue of S-modulin in frog retina. J Biol Chem. 1996; 271:21359–21364. [PubMed: 8702916]

Kawamura S. Calcium-dependent regulation of rhodopsin phosphorylation. Novartis Found Symp. 1999; 224:208–218. discussion 218–224. [PubMed: 10614053]

Kawamura S, Tachibanaki S. S-modulin. Adv Exp Med Biol. 2002; 514:61–68. [PubMed: 12596915]

Kefalov V, Fu Y, Marsh-Armstrong N, Yau KW. Role of visual pigment properties in rod and cone phototransduction. Nature. 2003; 425:526–531. [PubMed: 14523449]

Kenkre JS, Moran NA, Lamb TD, Mahroo OA. Extremely rapid recovery of human cone circulating current at the extinction of bleaching exposures. J Physiol. 2005; 567:95–112. [PubMed: 15932890]

Kennedy MJ, Dunn FA, Hurley JB. Visual pigment phosphorylation but not transducin translocation can contribute to light adaptation in zebrafish cones. Neuron. 2004; 41:915–928. [PubMed: 15046724]

Koch KW, Stryer L. Highly cooperative feedback control of retinal rod guanylate cyclase by calcium ions. Nature. 1988; 334:64–66. [PubMed: 2455233]

Koch KW, Duda T, Sharma RK. Photoreceptor specific guanylate cyclases in vertebrate phototransduction. Mol Cell Biochem. 2002; 230:97–106. [PubMed: 11952100]

Koenig D, Hofer H. The absolute threshold of cone vision. Journal of vision. 2011; 11

Korenbrot JI, Miller DL. Cytoplasmic free calcium concentration in dark-adapted retinal rod outer segments. Vision Res. 1989; 29:939–948. [PubMed: 2516928]

Korenbrot JI, Rebrik TI. Tuning outer segment Ca2+ homeostasis to phototransduction in rods and cones. Adv Exp Med Biol. 2002; 514:179–203. [PubMed: 12596922]

Korenbrot JI. Speed, adaptation, and stability of the response to light in cone photoreceptors: the functional role of Ca-dependent modulation of ligand sensitivity in cGMP-gated ion channels. J Gen Physiol. 2012; 139:31– 56. [PubMed: 22200947]

Koutalos Y, Nakatani K, Tamura T, Yau KW. Characterization of guanylate cyclase activity in single retinal rod outer segments. J Gen Physiol. 1995a; 106:863–890. [PubMed: 8648296]

Koutalos Y, Nakatani K, Yau KW. The cGMP-phosphodiesterase and its contribution to sensitivity regulation in retinal rods. J Gen Physiol. 1995b; 106:891–921. [PubMed: 8648297]

Kraft TW, Schneeweis DM, Schnapf JL. Visual transduction in human rod photoreceptors. J Physiol. 1993; 464:747–765. [PubMed: 8229828]

Krispel CM, Chen D, Melling N, Chen YJ, Martemyanov KA, Quillinan N, Arshavsky VY, Wensel TG, Chen CK, Burns ME. RGS expression rate-limits recovery of rod photoresponses. Neuron. 2006; 51:409–416. [PubMed: 16908407]

Kusnetzow A, Dukkipati A, Babu KR, Singh D, Vought BW, Knox BE, Birge RR. The photobleaching sequence of a short-wavelength visual pigment. Biochemistry. 2001; 40:7832–7844. [PubMed: 11425310]

Lagnado L, McNaughton PA. Net charge transport during sodium-dependent calcium extrusion in isolated salamander rod outer segments. J Gen Physiol. 1991; 98:479–495. [PubMed: 1722238]

Lagnado L, Cervetto L, McNaughton PA. Calcium homeostasis in the outer segments of retinal rods from the tiger salamander. J Physiol. 1992; 455:111–142. [PubMed: 1282928]

Lamb TD, McNaughton PA, Yau KW. Spatial spread of activation and background desensitization in toad rod outer segments. J Physiol. 1981; 319:463–496. [PubMed: 6798202]

Lamb TD. Effects of temperature changes on toad rod photocurrents. J Physiol. 1984; 346:557–578. [PubMed: 6422031]

Lamb TD, Arendt D, Collin SP. The evolution of phototransduction and eyes. Philos Trans R Soc Lond B Biol Sci. 2009; 364:2791–2793. [PubMed: 19720644]

Lambrecht HG, Koch KW. A 26 kd calcium binding protein from bovine rod outer segments as modulator of photoreceptor guanylate cyclase. EMBO J. 1991; 10:793–798. [PubMed: 1672637]

Lerea CL, Somers DE, Hurley JB, Klock IB, Bunt-Milam AH. Identification of specific transducin alpha subunits in retinal rod and cone photoreceptors. Science. 1986; 234:77–80. [PubMed: 3529395]

Lerea CL, Bunt-Milam AH, Hurley JB. Alpha transducin is present in blue-, green-, and red-sensitive cone photoreceptors in the human retina. Neuron. 1989; 3:367–376. [PubMed: 2534964]

Leskov IB, Klenchin VA, Handy JW, Whitlock GG, Govardovskii VI, Bownds MD, Lamb TD, Pugh EN Jr, Arshavsky VY. The gain of rod phototransduction: reconciliation of biochemical and electrophysiological measurements. Neuron. 2000; 27:525–537. [PubMed: 11055435]

Leung YT, Fain GL, Matthews HR. Simultaneous measurement of current and calcium in the ultravioletsensitive cones of zebrafish. J Physiol. 2007; 579:15–27. [PubMed: 17124271]

Li XF, Kiedrowski L, Tremblay F, Fernandez FR, Perizzolo M, Winkfein RJ, Turner RW, Bains JS, Rancourt DE, Lytton J. Importance of K+-dependent Na+/Ca2+-exchanger 2, NCKX2, in motor learning and memory. J Biol Chem. 2006; 281:6273–6282. [PubMed: 16407245]

Liu J, Li GL, Yang XL. An ionotropic GABA receptor with novel pharmacology at bullfrog cone photoreceptor terminals. Neuro-Signals. 2006; 15:13–25. [PubMed: 16825800]

Liu YT, Matte SL, Corbin JD, Francis SH, Cote RH. Probing the catalytic sites and activation mechanism of photoreceptor phosphodiesterase using radiolabeled phosphodiesterase inhibitors. J Biol Chem. 2009; 284:31541–31547. [PubMed: 19758990]

Lolley RN, Racz E. Calcium modulation of cyclic GMP synthesis in rat visual cells. Vision Res. 1982; 22:1481– 1486. [PubMed: 6305024]

Lugnier C. Cyclic nucleotide phosphodiesterase (PDE) superfamily: a new target for the development of specific therapeutic agents. Pharmacol Ther. 2006; 109:366–398. [PubMed: 16102838]

Luo DG, Yue WW, Ala-Laurila P, Yau KW. Activation of visual pigments by light and heat. Science. 2011; 332:1307–1312. [PubMed: 21659602]

Lytton J. Na+/Ca2+ exchangers: three mammalian gene families control Ca2+ transport. Biochem J. 2007; 406:365–382. [PubMed: 17716241]

Mante V, Frazor RA, Bonin V, Geisler WS, Carandini M. Independence of luminance and contrast in natural scenes and in the early visual system. Nat Neurosci. 2005; 8:1690–1697. [PubMed: 16286933]

Maricq AV, Korenbrot JI. Calcium and calcium-dependent chloride currents generate action potentials in solitary cone photoreceptors. Neuron. 1988; 1:503–515. [PubMed: 2483100]

Maricq AV, Korenbrot JI. Potassium currents in the inner segment of single retinal cone photoreceptors. J Neurophysiol. 1990a; 64:1929–1940. [PubMed: 2074473]

Maricq AV, Korenbrot JI. Inward rectification in the inner segment of single retinal cone photoreceptors. J Neurophysiol. 1990b; 64:1917–1928. [PubMed: 1705964]

Matthews G. Spread of the light response along the rod outer segment: an estimate from patch-clamp recordings. Vision Res. 1986; 26:535–541. [PubMed: 3090779]

Matthews G. Single-channel recordings demonstrate that cGMP opens the light- sensitive ion channel of the rod photoreceptor. Proc Natl Acad Sci U S A. 1987; 84:299–302. [PubMed: 2432606]

Matthews HR, Fain GL, Murphy RL, Lamb TD. Light adaptation in cone photoreceptors of the salamander: a role for cytoplasmic calcium. J Physiol. 1990; 420:447–469. [PubMed: 2109062]

Matthews HR, Sampath AP. Photopigment quenching is Ca2+ dependent and controls response duration in salamander L-cone photoreceptors. J Gen Physiol. 2010; 135:355–366. [PubMed: 20231373]

McCarthy ST, Younger JP, Owen WG. Free calcium concentrations in bullfrog rods determined in the presence of multiple forms of Fura-2. Biophys J. 1994; 67:2076–2089. [PubMed: 7858145]

Mendez A, Burns ME, Roca A, Lem J, Wu LW, Simon MI, Baylor DA, Chen J. Rapid and reproducible deactivation of rhodopsin requires multiple phosphorylation sites. Neuron. 2000; 28:153–164. [PubMed: 11086991]

Menini, A. The neurobiology of olfaction. CRC Press; Boca Raton, Fl. USA: 2010.

Miller DL, Korenbrot JI. Kinetics of light-dependent Ca fluxes across the plasma membrane of rod outer segments. A dynamic model of the regulation of the cytoplasmic Ca concentration. J Gen Physiol. 1987; 90:397– 425. [PubMed: 3116153]

Miller JL, Korenbrot JI. Phototransduction and adaptation in rods, single cones, and twin cones of the striped bass retina: a comparative study. Vis Neurosci. 1993a; 10:653–667. [PubMed: 8338802]

Miller JL, Korenbrot JI. In retinal cones, membrane depolarization in darkness activates the cGMP-dependent conductance. A model of Ca homeostasis and the regulation of guanylate cyclase. J Gen Physiol. 1993b; 101:933–960. [PubMed: 8101210]

Miller JL, Korenbrot JI. Differences in calcium homeostasis between retinal rod and cone photoreceptors revealed by the effects of voltage on the cgmp-gated conductance in intact cells. J Gen Physiol. 1994; 104:909– 940. [PubMed: 7876828]

Muradov H, Boyd KK, Haeri M, Kerov V, Knox BE, Artemyev NO. Characterization of human cone phosphodiesterase-6 ectopically expressed in Xenopus laevis rods. J Biol Chem. 2009; 284:32662–32669. [PubMed: 19801642]

Muradov H, Boyd KK, Artemyev NO. Rod phosphodiesterase-6 PDE6A and PDE6B subunits are enzymatically equivalent. J Biol Chem. 2010; 285:39828–39834. [PubMed: 20940301]

Naarendorp F, Esdaille TM, Banden SM, Andrews-Labenski J, Gross OP, Pugh EN Jr. Dark light, rod saturation, and the absolute and incremental sensitivity of mouse cone vision. J Neurosci. 2010; 30:12495– 12507. [PubMed: 20844144]

Nakatani K, Yau KW. Calcium and light adaptation in retinal rods and cones. Nature. 1988; 334:69–71. [PubMed: 3386743]

Nakatani K, Yau KW. Sodium-dependent calcium extrusion and sensitivity regulation in retinal cones of the salamander. J Physiol. 1989; 409:525–548. [PubMed: 2479741]

Nakatani K, Tamura T, Yau KW. Light adaptation in retinal rods of the rabbit and two other nonprimate mammals. J Gen Physiol. 1991; 97:413–435. [PubMed: 2037836]

Nakatani K, Koutalos Y, Yau KW. Ca2+ modulation of the cGMP-gated channel of bullfrog retinal rod photoreceptor. J Physiol. 1995a; 484:69–76. [PubMed: 7541463]

Nakatani K, Koutalos Y, Yau KW. Ca2+ modulation of the cGMP-gated channel of bullfrog retinal rod photoreceptors. Journal of Physiology. 1995b; 484 (Pt 1):69–76. [PubMed: 7541463]

Neher E. The use of fura-2 for estimating Ca buffers and Ca fluxes. Neuropharmacology. 1995; 34:1423–1442. [PubMed: 8606791]

Nikonov S, Engheta N, Pugh EN Jr. Kinetics of recovery of the dark-adapted salamander rod photoresponse. J Gen Physiol. 1998; 111:7–37. [PubMed: 9417132]

Nikonov S, Lamb TD, Pugh EN Jr. The role of steady phosphodiesterase activity in the kinetics and sensitivity of the light-adapted salamander rod photoresponse. J Gen Physiol. 2000; 116:795–824. [PubMed: 11099349]

Nilsson DE, Arendt D. Eye evolution: the blurry beginning. Curr Biol. 2008; 18:R1096–1098. [PubMed: 19081043]

Noel JP, Hamm HE, Sigler PB. The 2.2 A crystal structure of transducin-alpha complexed with GTP gamma S. Nature. 1993; 366:654–663. [PubMed: 8259210]

Normann RA, Werblin FS. Control of retinal sensitivity. I Light and dark adaptation of vertebrate rods and cones. J Gen Physiol. 1974; 63:37–61. [PubMed: 4359063]

Normann RA, Perlman I. The effects of background illumination on the photoresponses of red and green cones. J Physiol. 1979; 286:491–507. [PubMed: 439037]

Ohyama T, Hackos DH, Frings S, Hagen V, Kaupp UB, Korenbrot JI. Fraction of the dark current carried by Ca(2+) through cGMP-gated ion channels of intact rod and cone photoreceptors. J Gen Physiol. 2000; 116:735–754. [PubMed: 11099344]

Ohyama T, Picones A, Korenbrot JI. Voltage-dependence of ion permeation in Cyclic GMP-gated ion channels is optimized for cell function in rod and cone photoreceptors. J Gen Physiol. 2002; 119:341–354. [PubMed: 11929885]

Okawa H, Sampath AP, Laughlin SB, Fain GL. ATP consumption by mammalian rod photoreceptors in darkness and in light. Curr Biol. 2008; 18:1917–1921. [PubMed: 19084410]

Paillart C, Winkfein RJ, Schnetkamp PPM, Korenbrot JI. Functional characterization and molecular cloning of the K+-dependent Na+/Ca2+ exchanger in intact retinal cone photoreceptors. J Gen Physiol. 2007; 129:1–16. [PubMed: 17158950]

Palczewski K. G protein-coupled receptor rhodopsin. Ann Rev Biochem. 2006; 75:743–67. [PubMed: 16756510]

Park JH, Scheerer P, Hofmann KP, Choe HW, Ernst OP. Crystal structure of the ligand-free G-protein-coupled receptor opsin. Nature. 2008; 454:183–187. [PubMed: 18563085]

Pepperberg DR, Cornwall MC, Kahlert M, Hofmann KP, Jin J, Jones GJ, Ripps H. Light-dependent delay in the falling phase of the retinal rod photoresponse. Vis Neurosci. 1992; 8:9–18. [PubMed: 1739680]

Perlman I, Normann RA. Light adaptation and sensitivity controlling mechanisms in vertebrate photoreceptors. Prog Retin Eye Res. 1998; 17:523–563. [PubMed: 9777649]

Perry RJ, McNaughton PA. Response properties of cones of the retina of the tiger salamander. Journal Of Physiology. 1991; 433:561–587. [PubMed: 1841958]

Perry RJ, McNaughton PA. The mechanism of ion transport by the Na(+)-Ca2+,K+ exchange in rods isolated from the salamander retina. J Physiol. 1993; 466:443–480. [PubMed: 8410702]

Picones A, Korenbrot JI. Permeation and interaction of monovalent cations with the cGMP-gated channel of cone photoreceptors. J Gen Physiol. 1992; 100:647–673. [PubMed: 1334122]

Picones A, Korenbrot JI. Analysis of fluctuations in the cGMP-dependent currents of cone photoreceptor outer segments. Biophys J. 1994; 66:360–365. [PubMed: 8161689]

Picones A, Korenbrot JI. Permeability and interaction of Ca2+ with cGMP-gated ion channels differ in retinal rod and cone photoreceptors. Biophys J. 1995; 69:120–127. [PubMed: 7545443]

Plachetzki DC, Serb JM, Oakley TH. New insights into the evolutionary history of photoreceptor cells. Trends in ecology & evolution. 2005; 20:465–467. [PubMed: 16701418]

Plachetzki DC, Oakley TH. Key transitions during the evolution of animal phototransduction: novelty, “tree-thinking,” co-option, and co-duplication. Integr Comp Biol. 2007; 47:759–769. [PubMed: 21669757]

Plachetzki DC, Fong CR, Oakley TH. The evolution of phototransduction from an ancestral cyclic nucleotide gated pathway. Proc Biol Sci. 2010; 277:1963–1969. [PubMed: 20219739]

Pugh EN Jr, Lamb TD. Amplification and kinetics of the activation steps in phototransduction. Biochim Biophys Acta. 1993; 1141:111–149. [PubMed: 8382952]

Pugh EN Jr, Duda T, Sitaramayya A, Sharma RK. Photoreceptor guanylate cyclases: a review. Biosci Rep. 1997; 17:429–473. [PubMed: 9419388]

Rebrik TI, Korenbrot JI. In intact cone photoreceptors, a Ca2+-dependent, diffusible factor modulates the cGMP-gated ion channels differently than in rods. J Gen Physiol. 1998; 112:537–548. [PubMed: 9806963]

Rebrik TI, Kotelnikova EA, Korenbrot JI. Time course and Ca(2+) dependence of sensitivity modulation in cyclic GMP-gated currents of intact cone photoreceptors. J Gen Physiol. 2000; 116:521–534. [PubMed: 11004202]

Rebrik TI, Korenbrot JI. In intact mammalian photoreceptors, Ca^{2+}-dependent modulation of cGMP-gated ion channels is detectable in cones but not in rods. J Gen Physiol. 2004; 123:63–76. [PubMed: 14699078]

Rebrik TI, Botchkina I, Arshavsky VY, Craft CM, Korenbrot JI. CNG-Modulin: a novel Ca-dependent modulator of ligand sensitivity in cone photoreceptor cGMP-gated ion channels. J Neurosci. 2012a; 32:3142–3153. [PubMed: 22378887]

Rebrik, TI.; Mehta, M.; Tserentsoodol, N.; Hurley, JB.; Korenbrot, JI. CNG-modulin, the cone specific modulator of CNG channel activity, is required for the recovery of flash sensitivity under continuing illumination characteristic of cone photoreceptors; ARVO 2012 Meeting Abstracts; 2012b.

Reingruber J, Holcman D. The dynamics of phosphodiesterase activation in rods and cones. Biophys J. 2008; 94:1954–1970. [PubMed: 18065454]

Renninger SL, Gesemann M, Neuhauss SC. Cone arrestin confers cone vision of high temporal resolution in zebrafish larvae. Eur J Neurosci. 2011; 33:658–667. [PubMed: 21299656]

Rieke F, Baylor DA. Molecular origin of continuous dark noise in rod photoreceptors. Biophys J. 1996; 71:2553– 2572. [PubMed: 8913594]

Rieke F, Baylor DA. Origin of reproducibility in the responses of retinal rods to single photons. Biophys J. 1998; 75:1836–1857. [PubMed: 9746525]

Rieke F, Baylor DA. Origin and functional impact of dark noise in retinal cones. Neuron. 2000; 26:181–186. [PubMed: 10798402]

Rinner O, Makhankov YV, Biehlmaier O, Neuhauss SC. Knockdown of cone-specific kinase GRK7 in larval zebrafish leads to impaired cone response recovery and delayed dark adaptation. Neuron. 2005; 47:231–242. [PubMed: 16039565]

Sagoo MS, Lagnado L. The action of cytoplasmic calcium on the cGMP-activated channel in salamander rod photoreceptors. J Physiol. 1996; 497:309–319. [PubMed: 8961177]

Sakurai K, Onishi A, Imai H, Chisaka O, Ueda Y, Usukura J, Nakatani K, Shichida Y. Physiological properties of rod photoreceptor cells in green-sensitive cone pigment knock-in mice. J Gen Physiol. 2007; 130:21–40. [PubMed: 17591985]

Sampath AP, Matthews HR, Cornwall MC, Bandarchi J, Fain GL. Light-dependent changes in outer segment free-Ca2+ concentration in salamander cone photoreceptors. J Gen Physiol. 1999; 113:267–277. [PubMed: 9925824]

Sampath AP, Baylor DA. Molecular mechanism of spontaneous pigment activation in retinal cones. Biophys J. 2002; 83:184–193. [PubMed: 12080111]

Sato N, Kawamura S. Molecular mechanism of S-modulin action: binding target and effect of ATP. J Biochem. 1997; 122:1139–1145. [PubMed: 9498557]

Scheerer P, Park JH, Hildebrand PW, Kim YJ, Krauss N, Choe HW, Hofmann KP, Ernst OP. Crystal structure of opsin in its G-protein-interacting conformation. Nature. 2008; 455:497–502. [PubMed: 18818650]

Schnapf JL, Nunn BJ, Meister M, Baylor DA. Visual transduction in cones of the monkey macaca fascicularis [published erratum appears in j physiol (lond) 1990 dec;431:757]. J Physiol. 1990; 427:681–713. [PubMed: 2100987]

Schneeweis DM, Schnapf JL. The photovoltage of macaque cone photoreceptors: adaptation, noise, and kinetics. J Neurosci. 1999; 19:1203–1216. [PubMed: 9952398]

Schnetkamp PP, Szerencsei RT, Basu DK. Unidirectional Na+, Ca2+, and K+ fluxes through the bovine rod outer segment Na-Ca-K exchanger. J Biol Chem. 1991; 266:198–206. [PubMed: 1985893]

Schnetkamp PP. The SLC24 Na+/Ca2+-K+ exchanger family: vision and beyond. Pflugers Arch. 2004; 447:683–688. [PubMed: 14770312]

Scholten A, Koch KW. Differential calcium signaling by cone specific guanylate cyclase-activating proteins from the zebrafish retina. PloS one. 2011; 6:e23117. [PubMed: 21829700]

Schwab, IR. Evolution’s witness: how eyes evolved. Oxford University Press; New York: 2011.

Schwartz EA. Responses of single rods in the retina of the turtle. J Physiol. 1973; 232:503–514. [PubMed: 4759680]

Sesti F, Straforini M, Lamb TD, Torre V. Gating, selectivity and blockage of single channels activated by cyclic GMP in retinal rods of the tiger salamander. J Physiol. 1994; 474:203–222. [PubMed: 7516427]

Shen L, Caruso G, Bisegna P, Andreucci D, Gurevich VV, Hamm HE, DiBenedetto E. Dynamics of mouse rod phototransduction and its sensitivity to variation of key parameters. IET systems biology. 2010; 4:12– 32. [PubMed: 20001089]

Sheng JZ, Prinsen CF, Clark RB, Giles WR, Schnetkamp PP. Na(+)-Ca(2+)-K(+) currents measured in insect cells transfected with the retinal cone or rod Na(+)-Ca(2+)-K(+) exchanger cDNA. Biophys J. 2000; 79:1945–1953. [PubMed: 11023899]

Shichida Y, Morizumi T. Mechanism of G-protein activation by rhodopsin. Photochem Photobiol. 2007; 83:70– 75. [PubMed: 16800722]

Shuart NG, Haitin Y, Camp SS, Black KD, Zagotta WN. Molecular mechanism for 3:1 subunit stoichiometry of rod cyclic nucleotide-gated ion channels. Nature communications. 2011; 2:457.

Sneyd J, Tranchina D. Phototransduction in cones: an inverse problem in enzyme kinetics. Bull Math Biol. 1989; 51:749–784. [PubMed: 2573396]

Sondek J, Lambright DG, Noel JP, Hamm HE, Sigler PB. GTPase mechanism of Gproteins from the 1.7- A crystal structure of transducin alpha-GDP-AIF-4. Nature. 1994; 372:276–279. [PubMed: 7969474]

Sondek J, Bohm A, Lambright DG, Hamm HE, Sigler PB. Crystal structure of a G-protein beta gamma dimer at 2.1A resolution. Nature. 1996; 379:369–374. [PubMed: 8552196]

Soo FS, Detwiler PB, Rieke F. Light adaptation in salamander L-cone photoreceptors. J Neurosci. 2008; 28:1331–1342. [PubMed: 18256253]

Sung CH, Chuang JZ. The cell biology of vision. J Cell Biol. 2010; 190:953–963. [PubMed: 20855501]

Tachibanaki S, Arinobu D, Shimauchi-Matsukawa Y, Tsushima S, Kawamura S. Highly effective phosphorylation by G protein-coupled receptor kinase 7 of light-activated visual pigment in cones. Proc Natl Acad Sci U S A. 2005; 102:9329–9334. Epub 2005 Jun 9315. [PubMed: 15958532]

Takemoto N, Tachibanaki S, Kawamura S. High cGMP synthetic activity in carp cones. Proc Natl Acad Sci U S A. 2009; 106:11788–11793. [PubMed: 19556550]

Tamura T, Nakatani K, Yau KW. Light adaptation in cat retinal rods. Science. 1989; 245:755–758. [PubMed: 2772634]

Tanaka JC, Furman RE. Divalent effects on cgmp-activated currents in excised patches from amphibian photoreceptors. J Memb Biol. 1993; 131:245–256.

Tatsukawa T, Hirasawa H, Kaneko A, Kaneda M. GABA-mediated component in the feedback response of turtle retinal cones. Vis Neurosci. 2005; 22:317–324. [PubMed: 16079007]

Thuilier G, Herse M, labs D, Foujols T, Peetermans W, Gillotay D, Simon PC, Manderl H. The solar spectral irradiance from 200 to 2400 nm as measured by the Solspec spectrometer from the Atlas and Eureca missions. Solar Physics. 2003; 214:1–22.

Tomita T. Genesis of photoreceptor potential. Vision Res. 1971; 11:1195. [PubMed: 5156790]

Torre V, Forti S, Menini A, Campani M. Model of phototransduction in retinal rods. Cold Spring Harbor Symp Quantit Biol. 1990; 55:563–573.

Tranchina D, Sneyd J, Cadenas ID. Light adaptation in turtle cones. Testing and analysis of a model for phototransduction. Biophys J. 1991; 60:217–237. [PubMed: 1653050]

Vishnivetskiy SA, Raman D, Wei J, Kennedy MJ, Hurley JB, Gurevich VV. Regulation of arrestin binding by rhodopsin phosphorylation level. J Biol Chem. 2007; 282:32075–32083. [PubMed: 17848565]

Vought BW, Dukkipatti A, Max M, Knox BE, Birge RR. Photochemistry of the primary event in short-wavelength visual opsins at low temperature. Biochemistry. 1999; 38:11287–11297. [PubMed: 10471278]

Vu TQ, McCarthy ST, Owen WG. Linear transduction of natural stimuli by dark-adapted and light-adapted rods of the salamander, Ambystoma tigrinum. J Physiol. 1997; 505 (Pt 1):193–204. [PubMed: 9409482]

Wada Y, Sugiyama J, Okano T, Fukada Y. GRK1 and GRK7: Unique cellular distribution and widely different activities of opsin phosphorylation in the zebrafish rods and cones. J Neurochem. 2006; 98:824–837. Epub 2006 Jun 2019. [PubMed: 16787417]

Weiergraber OH, Senin II, Philippov PP, Granzin J, Koch KW. Impact of N-terminal myristoylation on the Ca2+-dependent conformational transition in recoverin. J Biol Chem. 2003; 278:22972–22979. [PubMed: 12686556]

Weiss ER, Ducceschi MH, Horner TJ, Li A, Craft CM, Osawa S. Species-specific differences in expression of G-protein-coupled receptor kinase GRK 7 and GRK1 in mammalian cone photoreceptor cells: implications for cone cell phototransduction. J Neurosci. 2001; 21:9175–9184. [PubMed: 11717351]

Weitz D, Ficek N, Kremmer E, Bauer PJ, Kaupp UB. Subunit stoichiometry of the CNG channel of rod photoreceptors. Neuron. 2002; 36:881–889. [PubMed: 12467591]

Wells GB, Tanaka JC. Ion selectivity predictions from a two-site permeation model for the cyclic nucleotide-gated channel of retinal rod cells. Biophys J. 1997; 72:127–140. [PubMed: 8994598]

Wensel TG. Signal transducing membrane complexes of photoreceptor outer segments. Vision Res. 2008; 48:2052–2061. [PubMed: 18456304]

Whitlock GG, Lamb TD. Variability in the time course of single photon responses from toad rods: termination of rhodopsin's activity. Neuron. 1999; 23:337–351. [PubMed: 10399939]

Wu Q, Chen C, Koutalos Y. Longitudinal diffusion of a polar tracer in the outer segments of rod photoreceptors from different species. Photochem Photobiol. 2006; 82:1447–1451. [PubMed: 16906792]

Yau KW, Lamb TD, Matthews G, Baylor DA. Current fluctuations across single rod outer segments. Vision Res. 1979a; 19:387–390. [PubMed: 473606]

Yau KW, Matthews G, Baylor DA. Thermal activation of the visual transduction mechanism in retinal rods. Nature. 1979b; 279:806–807. [PubMed: 109776]

Yau KW, Nakatani K. Light-suppressible, cyclic GMP-sensitive conductance in the plasma membrane of a truncated rod outer segment. Nature. 1985a; 317:252–255. [PubMed: 2995816]

Yau KW, Nakatani K. Light-induced reduction of cytoplasmic free calcium in retinal rod outer segment. Nature. 1985b; 313:579–582. [PubMed: 2578628]

Yau KW, Baylor DA. Cyclic GMP-activated conductance of retinal photoreceptor cells. Annu Rev Neurosci. 1989; 12:289–327. [PubMed: 2467600]

Yoshizawa T. Molecular basis for color vision. Biophysical chemistry. 1994; 50:17–24. [PubMed: 8011932]

Younger JP, McCarthy ST, Owen WG. Light-dependent control of calcium in intact rods of the bullfrog Rana catesbeiana. J Neurophysiol. 1996; 75:354–366. [PubMed: 8822563]

Zhang X, Wensel TG, Kraft TW. GTPase regulators and photoresponses in cones of the eastern chipmunk. J Neurosci. 2003; 23:1287–1297. [PubMed: 12598617]

Zhang X, Cote RH. cGMP signaling in vertebrate retinal photoreceptor cells. Front Biosci. 2005; 10:1191–1204. [PubMed: 15769618]

Zhang X, Wensel TG, Yuan C. Tokay gecko photoreceptors achieve rod-like physiology with cone-like proteins. Photochem Photobiol. 2006; 82:1452–1460. [PubMed: 16553462]

Zheng J, Trudeau MC, Zagotta WN. Rod cyclic nucleotide-gated channels have a stoichiometry of three CNGA1 subunits and one CNGB1 subunit. Neuron. 2002; 36:891–896. [PubMed: 12467592]

Zhong H, Molday LL, Molday RS, Yau KW. The heteromeric cyclic nucleotide-gated channel adopts a 3A:1B stoichiometry. Nature. 2002; 420:193–198. [PubMed: 12432397]

Zhu X, Li A, Brown B, Weiss ER, Osawa S, Craft CM. Mouse cone arrestin expression pattern: light induced translocation in cone photoreceptors. Mol Vis. 2002a; 8:462–471. [PubMed: 12486395]

Zhu X, Ma B, Babu S, Murage J, Knox BE, Craft CM. Mouse cone arrestin gene characterization: promoter targets expression to cone photoreceptors. FEBS Lett. 2002b; 524:116–122. [PubMed: 12135752]

Zimmerman AL, Baylor DA. Cyclic GMP-sensitive conductance of retinal rods consists of aqueous pores. Nature. 1986; 321:70–72. [PubMed: 2422559]

Zimmerman AL, Baylor DA. Cation interactions within the cyclic GMP-activated channel of retinal rods from the tiger salamander. J Physiol. 1992; 449:759–783. [PubMed: 1381754]

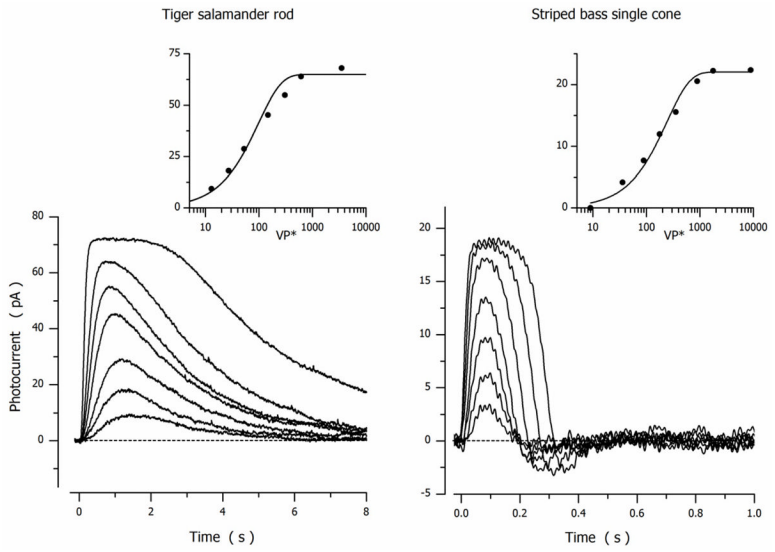

Figure 1.

Photocurrents measured at room temperature under voltage clamp in dark-adapted tiger salamander rods (holding voltage −30 mV) and striped bass single cones (holding voltage −40 mV). For the rod, 20 msec flashes delivered at time zero excited 13, 27, 53, 146, 307 and 614 rhodopsin molecule (λmax 520 nm) (Miller and Korenbrot, 1994). For the cone, 10 msec flashes delivered at time zero excited 35, 89, 178, 355, 892, 1780 and 3552 green opsin molecules (λmax 542 nm) (Korenbrot, 2012b).

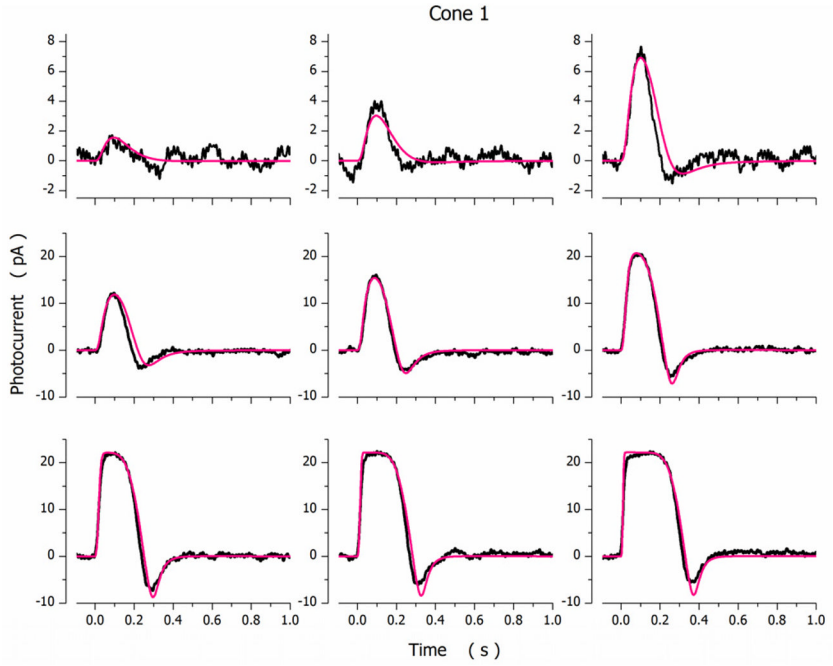

Figure 2.

Experimental (noisy, black traces) and simulated (noiseless, red traces) photocurrents measured under voltage-clamp at −40 mV in a dark adapted bass single cone. Photocurrents were elicited by 10 msec light flashes of intensity: 36, 71, 167, 356, 710, 1744, 3561, 7106 and 17443 VP*. For the cell *Ipeak*=22.2 pA and σ=170 VP*.

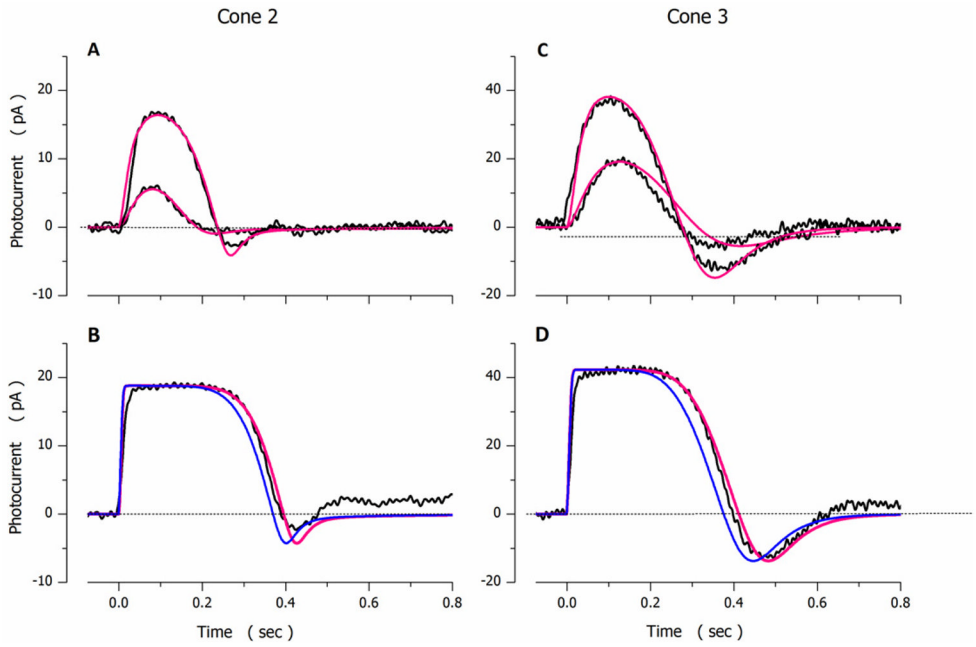

Figure 3.

Experimental (noisy, black traces) and simulated (noiseless, red traces) photocurrents measured in different dark adapted bass single cones. **A** and **B** were measured in one cell (*Ipeak*=19.1 pA and σ=195 VP*). **C** and **D** in another (*Ipeak*=42 pA and σ=112 VP*). Flash intensities tested were **A** 174 and 1747 VP*, **B** 17743 VP*, **C** 173 and 808 VP* and **D** 7720 VP* in. The values of the parameters used to compute the simulated data are listed in Table 3. At intensities above amplitude saturation (panels B and D) simulations fit experimental data only if PDE* inactivation was rate limited by VP* phosphorylation and this rate was slower than that during non-saturating responses (Table 3). The simulations illustrated in blue are computed without adjusting γ_{max}, maintaining the value used to fit the dim light responses.

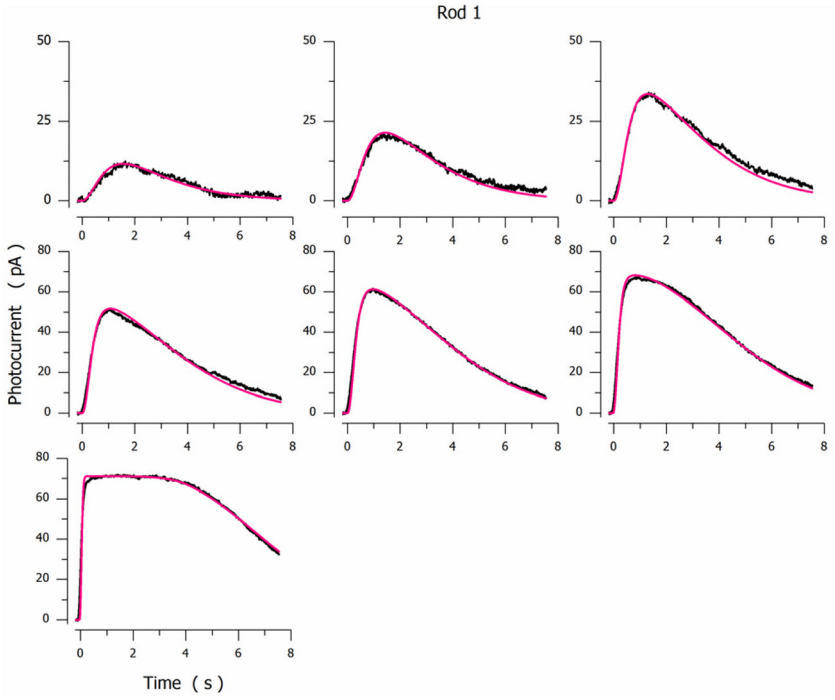

Figure 4.

Experimental (noisy, black traces) and simulated (noiseless, red traces) photocurrents measured under voltage-clamp at −30 mV in a dark adapted tiger salamander rod. Photocurrents were elicited by 20 msec light flashes of intensity: 13, 27, 53, 147, 307, 614 and 3509 VP*. *Ipeak*=72 pA, σ=62 Rh*.

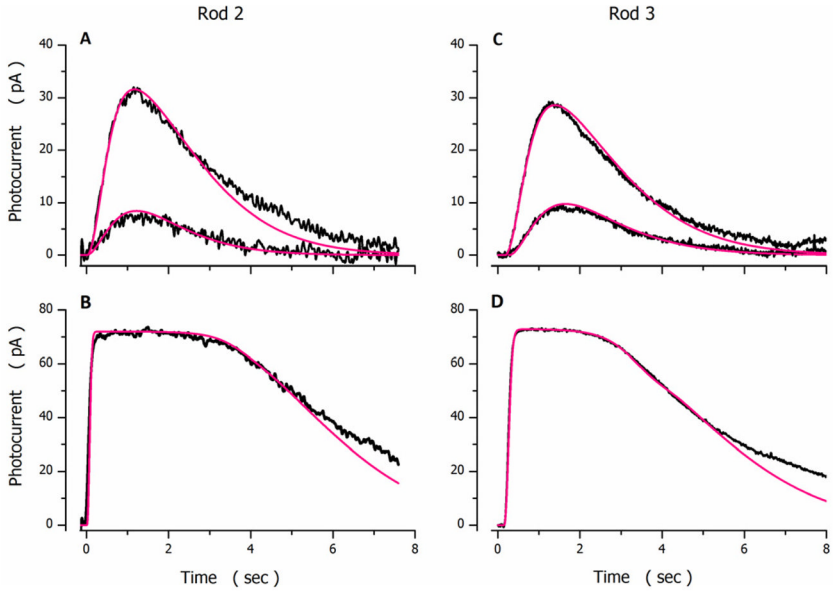

Figure 5.

Experimental (noisy, black traces) and simulated (noiseless, red traces) photocurrents measured in different dark-adapted tiger salamander rods. **A** and **B** were measured in one cell (*Ipeak*=74 pA and σ=59 Rh*) **C** and **D** in another (*Ipeak*=73 pA and σ=85.8 Rh*). Flash intensities tested were: **A** 13 and 53 VP*, **B** 5871 VP*; **C** 13 and 53 VP* and **D** 3509 VP*. The values of the parameters used to compute the simulated data are listed in Table 4.

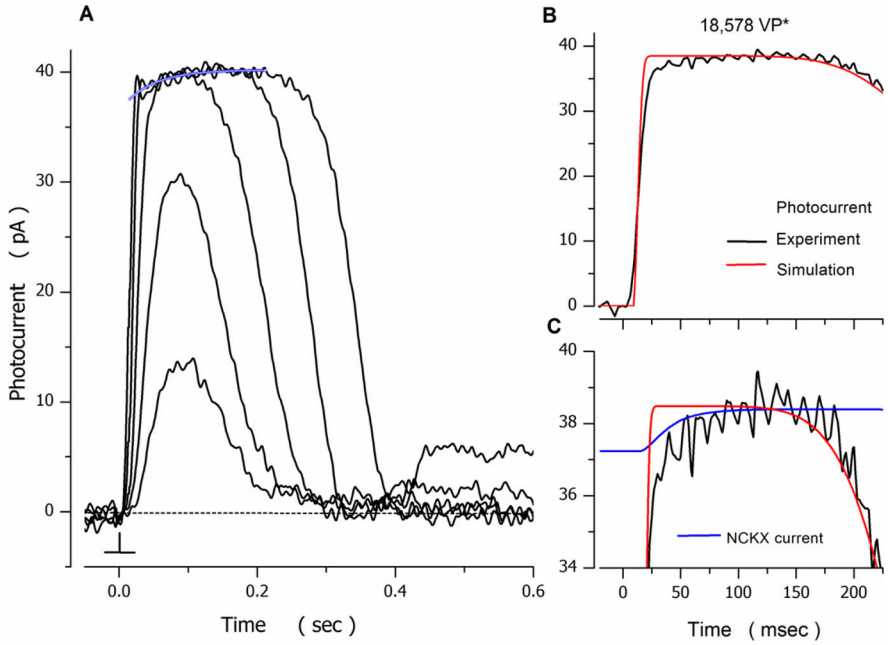

Figure 6.

Photocurrents in striped bass isolated single cones. **A**. Voltage-clamped photocurrents measured at −40 mV at room temperature. 10 msec duration flashes of 540 nm light were delivered at time zero. Intensity of the flashes tested was (in VP*): 175, 705, 4121, 18578 and 74648 respectively. At intensities sufficient to saturate photocurrent amplitude, the current approached saturation along a time course described by a single exponential process (blue tracing), of initial amplitude 2 pA and time constant τ_{NCKX} = 45 msec.
B and C. Experimental and simulated data activated by 18578 VP*, selected from panel A. **B**. Experimental (noisy, black trace) and simulated (noiseless, red trace) photocurrents. **C**. Experimental photocurrent (noisy, black traces) and the electrogenic Na^+/Ca^{2+}, K^+ exchanger current, I_{NCKX} (noiseless blue line) in an expanded view near photocurrent amplitude saturation. I_{NCKX} is as an explicit component of the simulated photocurrent that best fit the experimental current, as shown in B. I_{NCKX} is outward, but its display is inverted and offset to overlap with the photocurrent: its goes from a high value of 1.4 pA in the dark to zero, when photocurrent amplitude saturates.

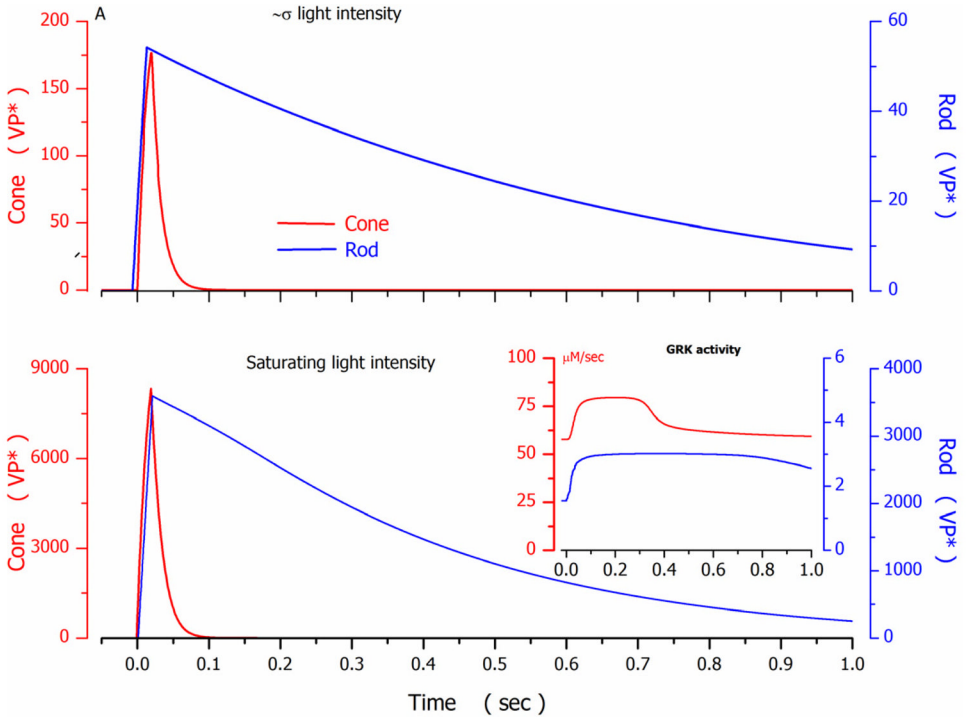

Figure 7.

Simulated time course of existence of excited visual pigment molecules (VP*) generated by flash stimulation. Panel **A** illustrates the number of VP* molecules in cone1 ( ) and rod1 ( ) in response to flashes near the intensity that half-saturates the photocurrent amplitude, 167 VP* in the cone and 53 VP* in the rod. Panel **B** illustrates the response to flashes that saturate the photocurrent amplitude, 7106 VP* in the cone and 3509 VP* in the rod. The inset in panel **B** illustrates the magnitude and time course of VP kinase catalytic activity in response to the bright flash stimulus.

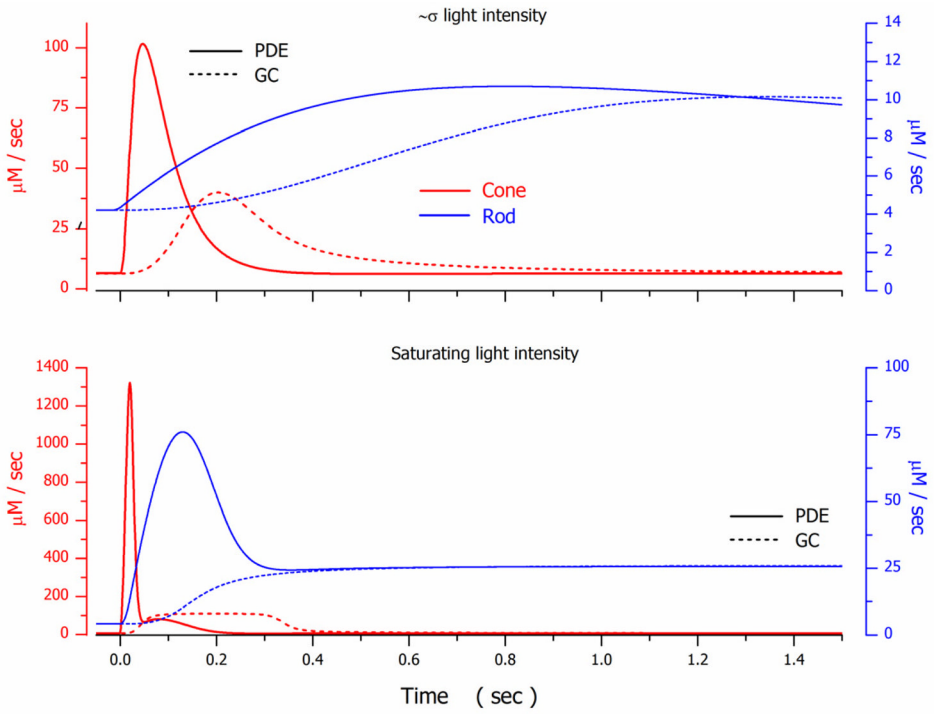

Figure 8.

Simulated time course of activation and inactivation of PDE* (▬) and GC (■ ■ ■ ■) in response to flash stimulation. Panel **A** illustrates enzymatic activity in response to flashes near the intensity that half-saturates the photocurrent amplitude, 167 VP* in cone 1 (▬) 53 VP* in rods 1 (▬). Panel **B** illustrates the response to flashes that saturate the photocurrent amplitude, 7106 VP* in the cone and 3509 VP* in the rod.

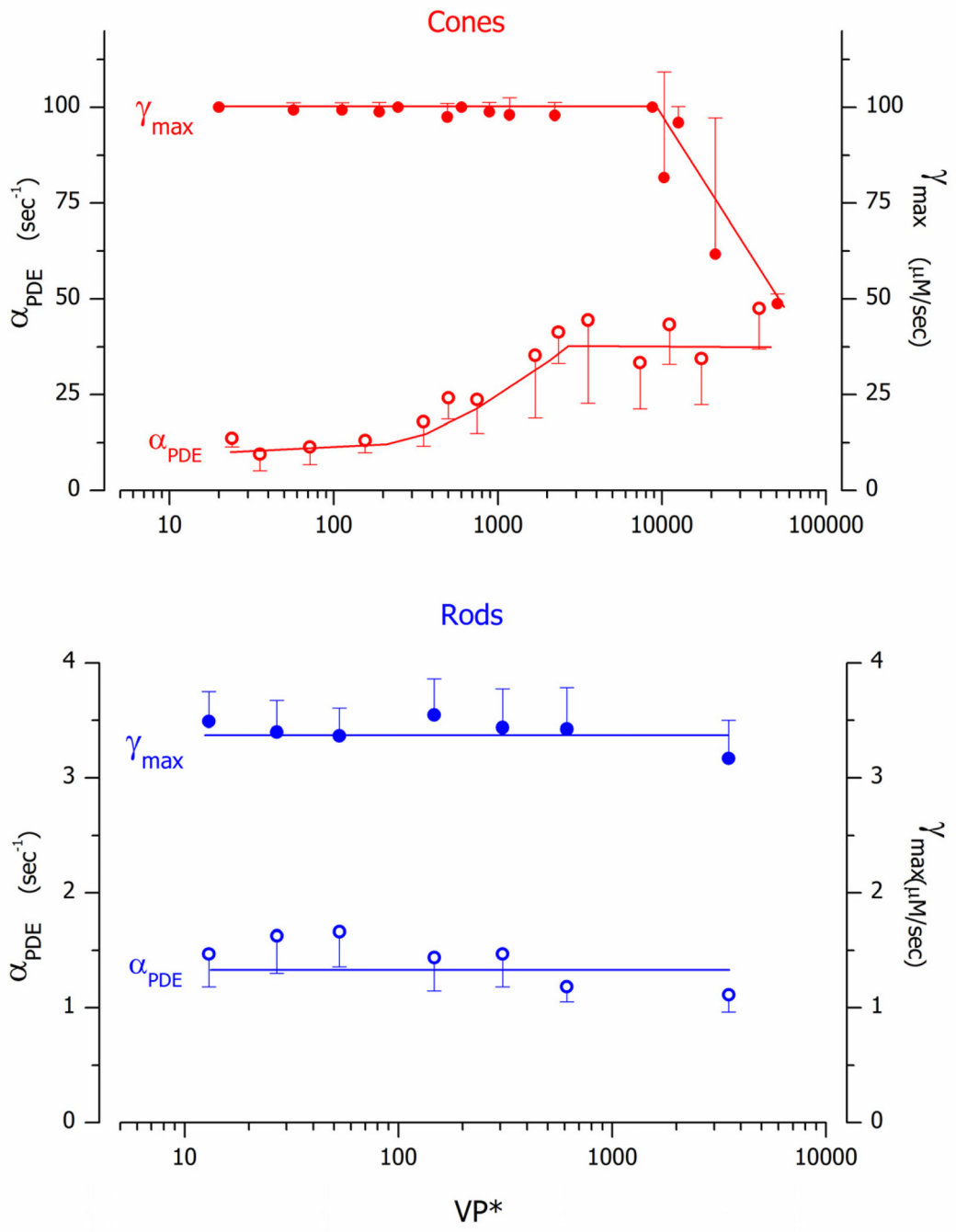

Figure 9.

Light-dependence of the simulated rate of PDE inactivation α_{PDE} (○) and VP kinase maximum activity γ_{max} (●) in cone 1 (▬) and rod 1 (▬). Shown are the mean ± SD. The continuous lines that join data points are drawn by eye.

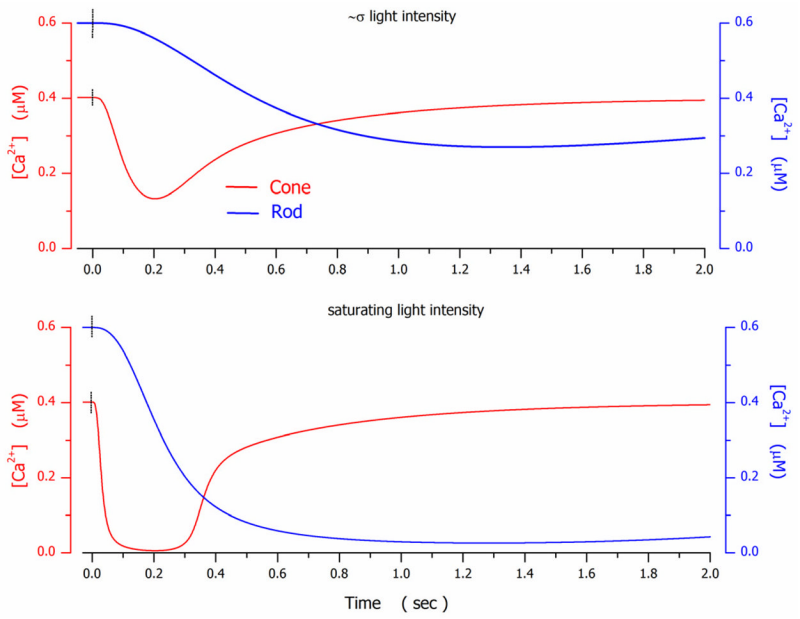

Figure 10.

Simulated time course of changes in cytoplasmic free Ca^{2+} concentration) generated by flash stimulation. Panels **A and B** illustrates the changes in cone 1 (▬) and rod 1 (▬) in response to flashes near the intensity that half-saturates the photocurrent amplitude, 167 VP* in the cone and 53 VP* in the rod. Same data are displayed with two different time scales to highlight differences in time course between rods and cones.

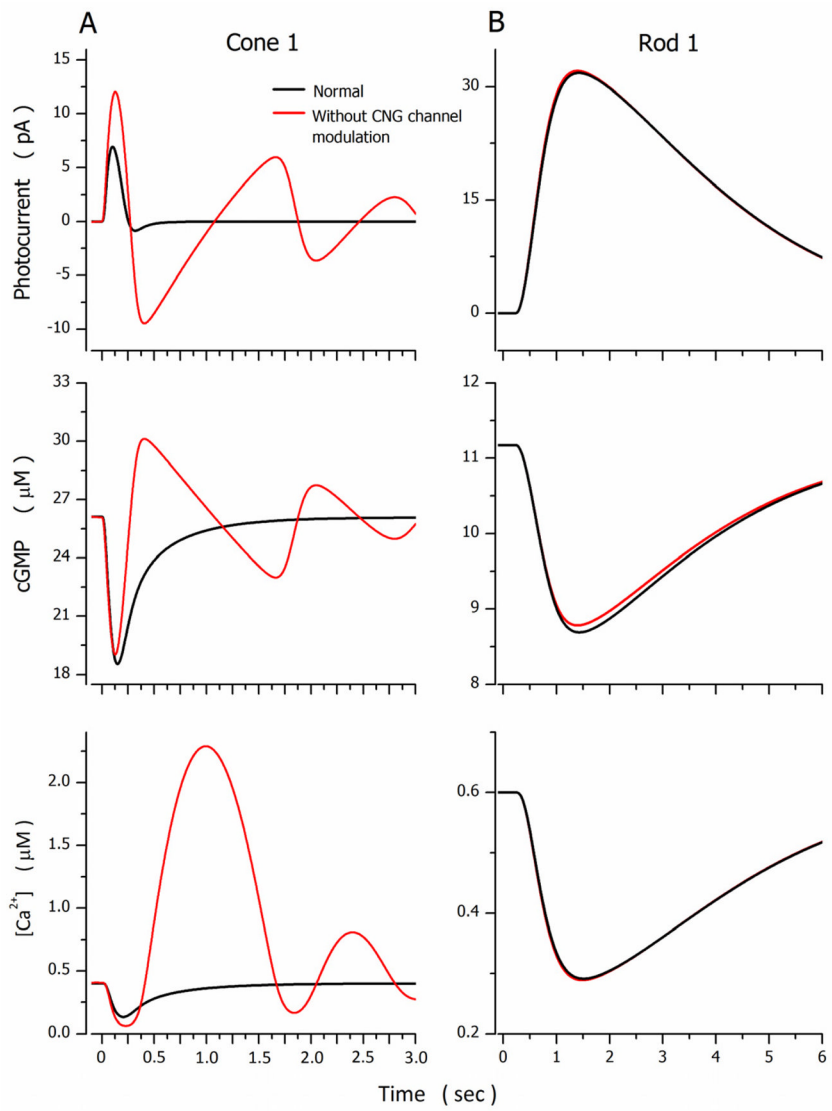

Figure 11.

Simulated changes in photocurrent, cytoplasmic cGMP concentration and cytoplasmic free Ca^{2+} generated by flash stimulation. Panel **A** illustrates the responses in cone1 to a flash 167 VP* in intensity, Panel **B** illustrates the responses in rod 1 to a 53 VP* intensity flash. In each panel are illustrated the responses in a normal photoreceptor (▬) and those in a model in which Ca^{2+}-dependent modulation of CNG channel ligand sensitivity is absent (▬).

Table 1

Model parameter values that best simulate dark current in rods and cones[a]

	Parameters	Units	[b] Cones	[c] Rods
CNG ion channel	I_{dark}	pA	27.3 ± 10.5	70.1 ± 18.9
	$cGMP_{dark}$	μM	[d]27.9 ± 14.2	10.9 ± 1.6
PDE	$^{dark}V_{PDE}$	μM/sec	[e]6.5 ± 1.48	4.26 ± 1.0
	K_m	μM	[f]26	10
	ε_{dark}	μM/sec	[g]12.6 ± 0.9	8.2 ± 1.9
GC	$^{dark}V_{GC}$	μM/sec	[h]6.5 ± 1.48	4.26 ± 1.0
Ca^{2+} influx	$^{in}J_{Ca}^{dark}$	μM/sec	[i]15 ± 5.8	16.3 ± 4.3
	P_f		[j]0.34	0.14
Ca^{2+} efflux	$^{out}J_{Ca}^{dark}$	μM/sec	[k]15 ± 5.8	16.3 ± 4.3
Free $[Ca^{2+}]$		μM	[l]0.4	0.6

[a] Values listed are referred to as “statistical”. They were measured experimentally in each and every one of the cells under investigation and the results averaged.

[b] Striped bass single cones, mean ± SD, N=18.

[c] Tiger salamander rods, mean ± SD, N=20.

[d] Computed from the circulating dark current (Text equations (1.1) and (1.2). Imax=2500 pA in cones (Rebrik et al., 2000), 1500 pA in rods (Hestrin and Korenbrot, 1987).

[e] Computed from the rate of dark current change when PDE or GC are suddenly and completely blocked, using text equations (1.1), (1.2) and the cytoplasmic free cGMP in the dark. The values listed are the mean of experimental measurements in intact tiger salamander rods (Hodgkin and Nunn, 1988; Koutalos et al., 1995b) and bass cones (Holcman and Korenbrot, 2005).

[f] Experimental data. In rods (Dumke et al., 1994b; Leskov et al., 2000; Muradov et al., 2010). In cones (Gillespie and Beavo, 1988; Muradov et al., 2010).

[g] From text equation (1.3).

[h] In darkness, GC and PDE enzymatic activities are the same.

[i] Computed from the circulating dark current. Text equation (1.6).

[j] Experimental data for both rods and cones (Ohyama et al., 2000).

[k] In darkness Ca^{2+} influx and efflux rate are the same.

[l] Assigned from experimental data. Rods (Gray-Keller and Detwiler, 1994; Younger et al., 1996). Cones (Sampath et al., 1999).

Table 2

Flash photosensitivity of dark adapted photoreceptors

	Single cones striped bass				Rods tiger salamander			
	I_{peak}	σ	*Threshold*	Time to peak	I_{peak}	σ	*Threshold*	Time to peak
	pA	VP*	VP*	msec	pA	VP*	VP*	msec
Mean	26.2	245.3	9.9	96.6	71	73	[b]1	1192.4
SEM	2.4	25.6	0.8	3.4	6.5	4.1		58.3
Cell count (N)	15	15	15	15	9	17		11
Minimum	16.5	101.9	4.6	70	40	43		865
Maximum	43.6	452.1	16.6	115	107	156		1531

Table 3

Model parameter values that best simulate flash photocurrents in dark adapted bass single cones[a]

	Parameters	Category	Units	Cone 1		Cone 2		Cone 3	
VP*	***Intensity***	**Statistical**	**VP***	**167**	**17,443**	**174**	**17,136**	**173**	**7,720**
GRK	γ_{max}	Adjustable	μM/sec	100	65	100	70	105	68
	μ_0	Invariant	μM/sec	0.5					
	ω_γ	Invariant		0.1					
T*	Ψ_0	Adjustable	1/sec	b_{230}		215		230	
	ω_{act}	Invariant		$c_{0.69}$					
PDE*	e_{sub}	Adjustable	μM/sec per molecule	$d_{0.185}$		0.323		0.416	
	α_{PDE}	Adjustable	1/sec	17.4	47	7	19	14	28
GC	V_{GC}^{max}	Invariant	μM/sec	$e_{110.5}$					
	${}^{GC}K_{Ca}$	Invariant	μM	0.1					
	n_{GC}	Invariant		2					
Ca^{2+} influx	${}^{in}J_{Ca}$	Statistical	μM/sec	25.3		37.5		17	
	P_f	Invariant		$f_{0.34}$					
Ca^{2+} buffer	K_{HA}	Adjustable	μM	$g_{0.030}$		0.044		0.091	
	C_{HA}	Adjustable	μM	21.4		4.6		66	
	B	Adjustable		10.6		7		15	
Ca^{2+} efflux	J_{Ca}^{max}	Statistical	pA	h_4		3.23		7.63	
	K_{Ca}^{exc}	Adjustable	μM	0.025		0.005		0.025	

[a] Values of parameters first used to compute dark current are not repeated here. They have the same values listed in Table 1.

[b] Experimental value is unknown in cones.

[c] Value from experimental data (Gibson et al., 2000). Experimental data available only for rhodopsin

[d] Text equation (2.13).

[e] Experimental value assigned from experimental measurements in truncated carp cones (Vmax = 140 uM/sec, (Takemoto et al., 2009)).

[f] Experimental value (Ohyama et al., 2000)

[g] Experimental mean values in aequorin-loaded rods are K_{HA} < 0.7 μM, C_{HA} 37 μM and B 16 (Lagnado et al., 1992). Experimental values are unknown in cones.

[h] With these values the computed mean time constant of Ca^{2+} clearance from bass cone outer segment when all CNG channels are suddenly closed is 40.0 ± 15.4 msec, similar to the experimental value of 43 ± 9.8 msec in the tiger salamander cone (Sampath et al, 1999)

Table 4

Model parameter values that best simulated flash photocurrents in dark adapted tiger salamander rods[a]

	Parameters	Category	Units	Rod 1		Rod 2		Rod 3	
VP*	***Intensity***	**Statistical**	**VP***	**53**	**3509**	**53**	**3509**	**53**	**3509**
GRK	γ_{max}	Adjustable	μM/sec	3.03		2.7	3.0	2.9	
	μ_0	Invariant	μM/sec	0.5					
	ω_γ	Invariant		0.1					
T*	Ψ_0	Adjustable	1/sec	b_{73}		80		62	
	ω_{act}	Invariant		$c_{0.69}$					
PDE*	ε_{sub}	Invariant	μM/sec per molecule	$d_{0.0083}$					
	k_{cat}		1/sec	e_{5*10^3}					
	α_{PDE}	Adjustable	1/sec	$f_{0.59}$		1.0	0.83	0.89	0.78
GC	V_{GC}^{max}	Adjustable	μM/sec	$g_{26.1}$		26.2		26.4	
	GCK_{Ca}	Invariant	μM	0.2					
	n_{GC}	Invariant		1.5					
Ca_{2+} influx	${}^{in}J_{Ca}$	Statistical	μM/sec	19.5		16.8		13.1	
	P_f	Invariant		$h_{0.14}$					
Ca_{2+} buffer	K_{HA}	Adjustable	μM	$i_{0.056}$					
	C_H	Adjustable	μM	5		8.5		8	
	B	Adjustable		1		1		2	
Ca_{2+} efflux max	J_{Ca}^{max}	Statistical	pA	18.3		18.5		18.74	
	K_{Ca}^{exc}	Invariant	μM	$j_{1.6}$					

[a] Values of parameters first used to compute dark current are not repeated here. They have the same values listed in Table 1.

[b] Ψ_0 experimental mean value in rods is ~100 sec^{-1} (Leskov et al., 2000).

[c] Experimental data (Gibson et al., 2000).

[d] The ε_{sub} value superficially appears to be 10-fold higher than the β_{sub} value experimentally measured by Leskov et al. (2000) and frequently quoted. However, both values reflect the same PDE hydrolytic activity, k_{cat}, they are simply defined in different units.

[e] Assigned k_{cat} value measured in biochemical assays' [(Dumke et al., 1994a; D'Amours and Cote, 1999; Zhang et al., 2003; Muradov et al., 2009). ε_{sub} is calculated from this assigned value and the salamander rod outer segment cytoplasmic volume (1 pL)

[f] Similar to experimental time constant measured in truncated toad rod outer segments (~ 2 ec)(Rieke and Baylor, 1998)

[g] The same parameter has the value 13 μM/sec in truncated frog rods (Koutalos et al., 1995a) and 29 μM/sec in truncated carp rods (Takemoto et al., 2009)

[h] Experimental value (Ohyama et al., 2000).

[i] Experimental mean values are $K_{HA} \ll 0.7$ μM, C_{HA} 37 μM and B 16 (Lagnado et al., 1992).

[j] Assigned from the experimentally known value (Lagnado et al., 1992; Sheng et al., 2000).

Table 5

Summary comparison of model parameter values in rods and cones

	Parameters	Units	[a] Cone	[b] Rod
CNG channels	$^{min}K_{cG}$	μM	120.6 ± 9.3	28 ± 6
	$^{max}K_{cG}$	μM	316 ± 43	37 ± 8
	K_{Ca}	μM	0.863 ± 0.051	0.055 ± 0.013
	n_{CNG}		2.5	2.3
GRK	γ_{max}	μM/sec	See Figure 9	See Figure 9
	μ_0	μM/sec	0.5	
	ω_γ		0.1	
T	Ψ_0	1/sec	231 ± 19	85 ± 17
	ω_{act}		0.69	
PDE	e_{sub}	μM/sec	[c]0.334 ± 0.091	0.00837
	k_{cat}	1/sec	10×10^3	5×10^3
	α_{PDE}	1/sec	See Figure 9	See Figure 9
GC	V_{GC}^{max}	μM/sec	110.5	25.9 ± 2.9
	$^{GC}K_{Ca}$	μM	0.1	0.2
	n_{GC}		2	1.5
Ca^{2+} influx	P_f		0.34	0.14
Ca^{2+} buffer	K_{HA}	μM	0.052 ± 0.025	0.056 ± 0.017
	C_{HA}	μM	20.9 ± 12.9	7.3 ± 2.9
	B		11.5 ± 3.9	1.2 ± 0.4
Ca^{2+} efflux	I_{NCKX}^{max}	pA	4.87 ±1.88	18.2 ± 4.8
	K_{Ca}^{exc}	μM	[h]0.019 ± 0.009	1.6

[a] Striped bass single cones, mean ± SD, N=18

[b] Tiger salamander rods, mean ± SD, N=9